



## Anomalous Hall effect in $3d/5d$ multilayers mediated by interface scattering and nonlocal spin conductivity

T. H. Dang, Q. Barbedienne, D. Q. To, E. Rongione, N. Reyren, F. Godel , S. Collin, J. M. George , and H. Jaffrès   
*Unité Mixte de Physique CNRS/Thales, University Paris-Sud and Université Paris-Saclay, 91767 Palaiseau, France*

 (Received 22 January 2019; revised 20 July 2020; accepted 20 August 2020; published 2 October 2020)

We have evidenced unconventional anomalous Hall effects (AHEs) in  $3d/5d$  (Co0.2nm/Ni0.6nm)<sub>N</sub> multilayers grown on a thin Pt layer or thin Au:W alloys with perpendicular magnetic anisotropy (PMA) properties. The inversion of AHEs observed with one Pt series is explained by considering the opposite sign of the effective spin-orbit coupling of Pt compared to Co/Ni combined with peculiar specular electronic reflections. Using advanced simulations methods for the description of the spin-current profiles based on the spin-dependent Boltzmann formalism, we extracted the spin-Hall angle (SHA) of Pt and Co/Ni of opposite sign. The extracted SHA for Pt, +20%, is opposite to the one of Co/Ni, giving rise to an effective AHE inversion for thin Co/Ni multilayers (with the number of repetition layers  $N < 17$ ). The spin-Hall angle in Pt is found to be larger than the one previously measured by complementary spin-pumping inverse spin-Hall effect experiments in a geometry of current perpendicular to the plane. Whereas magnetic proximity effects cannot explain the effect, spin-current leakage and spin-orbit assisted electron scattering at Pt/(Co,Ni) interfaces fit the experiments. We also extract the main relevant electronic transport parameters governing the overall effects in current-in-plane (CIP) currents and demonstrate, in particular, that the specular/non-specularity in the electronic diffusion processes play an essential role to explain the observed results.

DOI: [10.1103/PhysRevB.102.144405](https://doi.org/10.1103/PhysRevB.102.144405)

### I. INTRODUCTION

In recent years, the field of *spin orbitronics* has emerged as a new route for spin currents able to generate spin torques and excite small magnetic elements [1–5], to move domain walls [6–12], to promote chiral Dzyaloshinskii-Moriya interactions (DMI) [7,13], or to generate THz waves probed by the time domain spectroscopy (THz-TDS) methods [14]. This is made possible via the so-called *intrinsic* spin-Hall effect (SHE) and reciprocal inverse spin-Hall effect (ISHE) [15–17] provided by heavy metals, e.g., Pt [18–22], Ta [2,3], and W [23], or via the *extrinsic* SHE of diluted metallic alloys investigated for their experimental properties [24–32] and from a theoretical point of view [33]. SHE borrows its concept from the well-established principles of the anomalous Hall effect (AHE) [15,16], whereby the relativistic spin-orbit interactions (SOIs) may promote an asymmetric deflection of the electron flow depending on their spin. Early studies of AHE mostly dealt with bulk ferromagnetic (FM) metals [34] and their alloys [35–39].

With the fast development of spin orbitronics, AHE has started to be largely investigated, from the early 1990s, in ultrathin multilayers such as Co/X, with X=Au [40], Pd [41–46], Pt [47,48], or, more recently, in Co/Ni multilayers [49] grown for their perpendicular magnetic anisotropy (PMA) properties [50] often required for magnetoelectronics devices. More recent experimental studies have exhibited the strong impact of the interfacial SOI on the injected spin current at heavy-metal/ferromagnetic-metal interfaces, thus promoting the necessary spin-orbit torques (SOTs) for mag-

netic commutation [51]. This reveals the need to use accurate analyses and anatomy of spin currents incorporating the spin-orbit degree of freedom.

To these ends, AHE and SHE involving  $3d$  transition metals (Fe, Co, Ni) or  $5d$  noble metals are presently the basis of numerous fundamental investigations dealing with an intrinsic mechanism originating from the Berry phase [34,52,53], skew-scattering diffusion processes [35,36,39,54–56], and extrinsic side-jump phenomena [37,38]. Moreover, very recent works have dealt with the specific role of the AHE of CoNi [57] and of NiFe [58] for magnetization controlled spin torques [59,60], the role of the electronic surface scattering on the properties of spin current for AHE, e.g., at the PtO<sub>x</sub>/Co interface [61], and the possible implication of the roughness on AHE for different related transition metal (TM) interfaces [62]. Examples of the relevance of such interface contribution are played by (i) the magnetic proximity effects in Pt at the scale of few atomic planes [63–66], as well as (ii) a possible spin-current depolarization or spin-memory loss (SML) at the  $3d/5d$  interface induced by local SOI, as suggested and discussed recently [19,51,66–69,100]. Regarding the issue of spin-current depolarization and its magnitude, another recent matter of debate is the typical value of the spin-Hall angle (SHA) of  $5d$  heavy metals such as Pt including both disorder [70] and SML at interfaces [71].

Nonetheless, much fewer works have dealt with multilayered systems wherein interfaces may bring new insights into the spin-orbit assisted electronic scattering and diffusions. Like AHE, the spin-dependent SHE properties are scaled by

the off-diagonal spin-dependent conductivity tensor  $\sigma_{xy}^s$  involving either intrinsic ( $\sigma_{xy}^{\text{int},s}$ ) [72] or extrinsic ( $\theta^{sk,s}\sigma_{xx}^s$ ) skew scattering, and extrinsic side-jump ( $\sigma_{xy}^{sj,s}$ ) contributions [16], with the result that

$$\sigma_{xy}^s = \sigma_{xy}^{\text{int},s} + \theta^{sk,s}\sigma_{xx}^s + \sigma_{xy}^{sj,s}, \quad (1)$$

where  $s$  is the  $\uparrow, \downarrow$  spin index, and where the subscripts ( $sk$ ), ( $sj$ ), ( $\text{int}$ ) denote, respectively, the *extrinsic skew scattering*, *extrinsic side-jump*, and *intrinsic* contributive terms [73]. In that framework, the off-diagonal conductivity term responsible for AHE, which is the *charge* contribution to AHE,  $\sigma_{xy}$ , is seen to be the sum of the two spin band channels,  $\sigma_{xy} = \sigma_{xy}^{\uparrow} + \sigma_{xy}^{\downarrow}$ , making the link between AHE and SHE that we are searching for. AHE and SHE in 3d ferromagnetic materials, as in Co [74,75] and Ni [76,77], are mainly expected to possess an *intrinsic* origin with opposite sign of  $\sigma_{xy}^{\text{int}}$ , as experimentally calculated and determined [78–81]. Nevertheless, the occurrence of exchange split Fermi surfaces in ferromagnets makes it generally difficult to extract a clear relationship between AHE and SHE. This particular feature has been debated in recent papers [54–56].

In the present work, we focus on the properties of AHE and on the control of the spin current in a *standard* perpendicular magnetic configuration with the magnetization standing along the  $z$  direction normal to the layers. Extensions could be made in the future to the case of the nonconventional situation of arbitrary magnetization direction within the ferromagnet [59,60]. We present unconventional results and refined analyses of nonlocal AHE in a series of Pt/(Co0.2nm/Ni0.6nm) $_N$  and Au : W/(Co0.2nm/Ni0.6nm) $_N$  multilayers (MLs) involving different numbers of Co/Ni sequences and corresponding interfaces. Co/Ni is known to possess a specific interface anisotropy exhibiting PMA [12,50,82] and, moreover, involving Dzyaloshinskii-Moriya interactions (DMI) [13,83]. By taking advantage of the relatively small AHE of (Co0.2/Ni0.6) $_N$  MLs and when  $N < 17$ , we demonstrate, in some specific situation, a sign change of the AHE in a series of ML structures grown onto the thin Pt buffer highlighted an opposite effective spin-orbit sign for Pt compared to Co/Ni. We use an advanced Boltzmann analysis algorithm for the necessary determination of the spin currents with adequate boundary conditions at interfaces and based on the extension of the Fuchs-Sondheimer approach [84], and like recently highlighted and exploited for Co/Ni multilayers [85]. It is based on the combination of electron scattering in multilayers [85,86] and SOI-assisted spin and charge deflection inside layers. The different contributions have been carefully addressed involving off-diagonal spin-flip terms in the diffusive potentials. We thus demonstrate that the AHE sign inversion originates from the nonlocal properties of the spin conductivities [30,71] and the opposite sign of the effective SOI strength compared to the bulk Co/Ni MLs more than induced magnetization in Pt [magnetic proximity effects (MPE)] [63–65]. Physical mechanisms of the nonlocal AHE effect in those systems rely thus on the combination of the SOI-dependent scattering of a polarized current generated in Co/Ni, specific electronic specularly reflections at interfaces [87–89], and the subsequent ISHE process in bulk adjacent heavy metal

(Pt, Au:W). This also reveals a characteristic large positive SHA (+20%) for Pt, at the Co/Pt interface that is much stronger [20,69,71] than previously determined in combined spin pumping–ISHE experiments [19] and that we may assign to an anisotropy in the scattering time [52,70]. By choosing consistent physical parameters, we find an excellent agreement with the experimental trends.

We have divided our paper into four different sections. Section II is devoted to the discussion of the sample preparation and experimental results dealing with Pt and Au:W buffer based multilayer Co/Ni samples. Section III is devoted to the description of the main modeling features governing the AHE and SHE phenomena, possibly incorporating *intrinsic* and *extrinsic* phenomena. We present detailed calculation methods that we used involving the spin-current profiles to model those effects in MLs before giving an accurate analysis of the data, emphasizing the importance of the specularly at interfaces, in Sec. IV. We give the main trends and conclusions in Sec. V.

## II. SAMPLE PREPARATION AND AHE EXPERIMENTS

Samples are deposited on thermally oxidized Si wafers of two types, respectively, I and II, at room temperature using magnetron sputtering. Type-I and type-II substrates differ by their level of roughness in the subnanometer scale, as discussed just below. Samples are made of a 6-nm-thick heavy-metal layer, i.e., Au:W alloys or Pt, covered by magnetic multilayers composed of  $N$  repetitions of Co 0.2 nm/Ni 0.6 nm bilayers with perpendicular magnetic anisotropy properties. Such Co/Ni stack is used to keep a large PMA about constant, at least up to  $N \cong 40\text{--}70$  in the present case, in order to preserve a low roughness at the surface or even more [50]. The resistivity  $\rho$  of Au:W thin films varies from 80 to 130  $\mu\Omega$  cm depending on the W content in the alloy, and we denote Au:W $_{\rho}$  as the Au:W alloy of resistivity  $\rho$  in  $\mu\Omega$  cm. The Pt bulk resistivity equals  $\rho_{\text{Pt}} = 17 \mu\Omega$  cm. All of the data and parameters are gathered in Table I, including those of Co, Ni, and Al materials within the stack. Devices are then patterned into Hall cross bars of different widths, ranging from 3 to 6  $\mu\text{m}$  and of 600  $\mu\text{m}$  length, by optical UV lithography and an Ar ion etching process. The samples are finally covered with a 5-nm-thick Al layer, hereafter oxidized onto 2 nm from the surface, to prevent oxidation of the Co/Ni stack. From previous work [29], we can infer that Pt and Au:W buffer layers possess the same or opposite spin-Hall angle (SHA) depending on the W content in Au:W and depending, thus, on its resistivity  $\rho_{\text{Au:W}}$ . According to our convention, the SHA is counted positive, which is of the same sign as that of Pt, for an Au:W alloy resistivity ( $\rho$ ) typically less than 110  $\mu\Omega$  cm, and it is counted negative, which is of the same sign as that of Ni or Co0.2/Ni0.6, for  $\rho > 120 \mu\Omega$  cm. For type-I Si substrates, atomic force microscopy (AFM) measurements allow one to determine an overall roughness of 0.3 nm root mean square (rms) at the 1  $\mu\text{m}$  scale for (Co/Ni) $_5$  and 1.3 nm rms for (Co/Ni) $_{20}$  samples. In contrast, for type-II Si substrates, the rms is about 0.3 nm for (Co/Ni) $_5$ , 0.36 nm for (Co/Ni) $_{20}$ , 0.7 nm for (Co/Ni) $_{70}$ , and 1.1 nm for (Co/Ni) $_{100}$ . Then, one must note that the rms between substrates of type I and II are not too different for  $N < 5$ , and then starts to strongly differ for  $N > 5$  up to  $N = 20\text{--}100$ . However, samples all keep their

TABLE I. Table of physical parameters of Pt, Co, and Ni extracted for type-II samples from our fit procedure in the case of pure *intrinsic* and *extrinsic* models for AHE. The error bar corresponds to the value of the latest significant figure.

Parameters	Symbols	Values for $\uparrow$ spin	Value for $\downarrow$ spin
Conductivity of Co	$\sigma_{\text{Co}}$ (S m <sup>-1</sup> )	$\frac{\sigma_{\text{Co}}}{1-\beta_{\text{Co}}} = 7.4 \times 10^6$	$\frac{\sigma_{\text{Co}}}{1+\beta_{\text{Co}}} = 2.7 \times 10^6$
Conductivity of Ni	$\sigma_{\text{Ni}}$ (S m <sup>-1</sup> )	$\frac{\sigma_{\text{Ni}}}{1-\beta_{\text{Ni}}} = 1.7 \times 10^7$	$\frac{\sigma_{\text{Ni}}}{1+\beta_{\text{Ni}}} = 2.3 \times 10^6$
Conductivity of Pt	$\sigma_{\text{Pt}}$ (S m <sup>-1</sup> )	$4.5 \times 10^6$ (S m <sup>-1</sup> )	$4.5 \times 10^6$ (S m <sup>-1</sup> )
Conductivity of Au:W <sub>130</sub>	$\sigma_{\text{Au:W}_{130}}$ (S m <sup>-1</sup> )	$3.85 \times 10^5$	$3.85 \times 10^5$
Conductivity of Au:W <sub>80</sub>	$\sigma_{\text{Au:W}_{80}}$ (S m <sup>-1</sup> )	$6.2 \times 10^5$	$6.2 \times 10^5$
Intrinsic Hall conductivity of Co/Ni [case (i)]	$\sigma_{xy}^{\text{int}}$ (S m <sup>-1</sup> )	$= \sigma_{xy}^{\text{int},\uparrow} + \sigma_{xy}^{\text{int},\downarrow} = -8.5 \times 10^3$ (S m <sup>-1</sup> )	
Mean free path of Co	$\lambda_{\text{Co}}$ (nm)	7.4	2.7
Mean free path of Ni	$\lambda_{\text{Ni}}$ (nm)	16	2.3
Mean free path of Pt	$\lambda_{\text{Pt}}$ (nm)	1.6	1.6
Mean free path of Au:W	$\lambda_{\text{Pt}}$ (nm)	0.4	0.4
Bulk asymmetry coefficient of Co	$\beta_{\text{Co}}$		0.46
Bulk asymmetry coefficient of Ni	$\beta_{\text{Ni}}$		0.76
Spin-Hall angle of Co/Ni [case (ii)]	$\theta_{\text{Co/Ni}}^{\uparrow}$	-0.9%	0
Spin-Hall angle of Co/Ni [case (iii)]	$\theta_{\text{Co/Ni}}^{\downarrow}$	0	2.2%
Spin-Hall angle of Co/Ni [case (iv)]	$\theta_{\text{Co/Ni}}$	-1.5%	1.5%
Spin-Hall angle of Pt	$\theta_{\text{Pt}}$	20%	-20%
Spin-Hall angle of Au:W <sub>130</sub>	$\theta_{\text{Au:W}_{130}}$	-0.3%	0.3%
Spin-Hall angle of Au:W <sub>80</sub>	$\theta_{\text{Au:W}_{130}}$	10%	-10%
Pt/Co average interface transmission	$t_{\text{Pt/Co}}$	$\frac{t_{\text{Pt/Co}}}{1-\gamma_{\text{Pt/Co}}} = 0.94$	$\frac{t_{\text{Pt/Co}}}{1+\gamma_{\text{Pt/Co}}} = 0.31$
Co/Ni average interface transmission	$t_{\text{Co/Ni}}$	$\frac{t_{\text{Co/Ni}}}{1-\gamma_{\text{Co/Ni}}} = 0.14$	$\frac{t_{\text{Co/Ni}}}{1+\gamma_{\text{Co/Ni}}} = 0.08$
Au:W/Co average interface transmission	$t_{\text{Au:W/Co}}$	$\frac{t_{\text{Au:W/Co}}}{1-\gamma_{\text{Au:W/Co}}} = 0.43$	$\frac{t_{\text{Au:W/Co}}}{1+\gamma_{\text{Au:W/Co}}} = 0.23$
Pt/Co interface asymmetry coefficient	$\gamma_{\text{Pt/Co}}$		0.5
Co/Ni interface asymmetry coefficient	$\gamma_{\text{Co/Ni}}$		0.9
Au:W/Co interface asymmetry coefficient	$\gamma_{\text{Au:W/Co}}$		0.3
Pt/Co specularity in reflection	$sP_{\text{Pt/Co}}$		0
Au:W/Co specularity in reflection	$sP_{\text{Au:W/Co}}$		0
Co/Ni specularity in reflection	$sP_{\text{Co/Ni}}$		0.4
Ni/Al specularity in reflection	$sP_{\text{Co/Ni}}$		0
Pt/Co spin-loss memory	$\delta_{\text{Pt/Co}}$		0.9
Co/Ni spin-loss memory	$\delta_{\text{Co/Ni}}$		0.3
Au:W/Co spin-loss memory	$\delta_{\text{Au:W/Co}}$		0

strong PMA properties, thus demonstrating the high quality of the nanometer scale interfaces, in particular free of large chemical intermixing.

We discuss below the main AHE results obtained on the different set of samples where a small ordinary Hall effect (OHE) has been subtracted in each case. OHE, preferentially revealed at low temperature (LT), will be briefly discussed hereafter and displayed in the Supplemental Material [90].

Figure 1 displays the AHE results obtained at room temperature (RT) on type-II samples (very flat) made of Au:W<sub>130</sub> 6 nm buffer of a large resistivity,  $\rho \simeq 130 \mu\Omega \text{ cm}$ , and characterized by a SHE sign opposite to the one of Pt [29]. Figure 1(a) shows the transverse resistance measurements, i.e., the AHE of the Au : W<sub>130</sub>6/(Co0.2/Ni0.6)<sub>40</sub> device with a large period repetition  $N = 40$  and corresponding to an overall Co,Ni thickness of 32 nm that we can consider as *bulk* Co/Ni. The AHE amplitude of  $\Delta R_{\text{AHE}} = -28 \text{ m}\Omega$  for  $N = 40$  gives a negative signature for the AHE of Ni, following our convention. This also remains true for Co/Ni MLs when

Ni, of a large intrinsic AHE, is thicker than Co and when  $N$  is sufficiently large for  $(\text{Co/Ni})_N$  to dominate the conduction process. From Fig. 1(b), the same conclusions holds for the samples grown on the 6 nm Au:W<sub>130</sub> buffer layers for  $N = 5$  associated, in proportion, to a larger current shunt in the Au:W<sub>130</sub>. The AHE amplitude is of the same sign (negative) and characterized by a larger amplitude,  $\Delta R_{\text{AHE}} = -80 \text{ m}\Omega$ , thus demonstrating the particular role of the buffer on the spin-current properties. This observation will be ascribed, via advanced calculation methods (Sec. IV), to a larger SHE angle of Au:W<sub>130</sub> compared to Co/Ni, and of the same sign, allowing thus a more efficient spin-charge conversion (AHE signal) of the spin-polarized current generated from the Co/Ni ferromagnetic layer.

In Figs. 2(a)–2(f), we report on the AHE acquired at RT provided with the same type-II sample series involving a Pt buffer. They are made of Pt 6 nm buffer with the number  $N$  of Co/Ni repetition layers within the  $N = 3$ –20 range and fabricated within the same batch. Figures 2(a) to 2(f) refer,

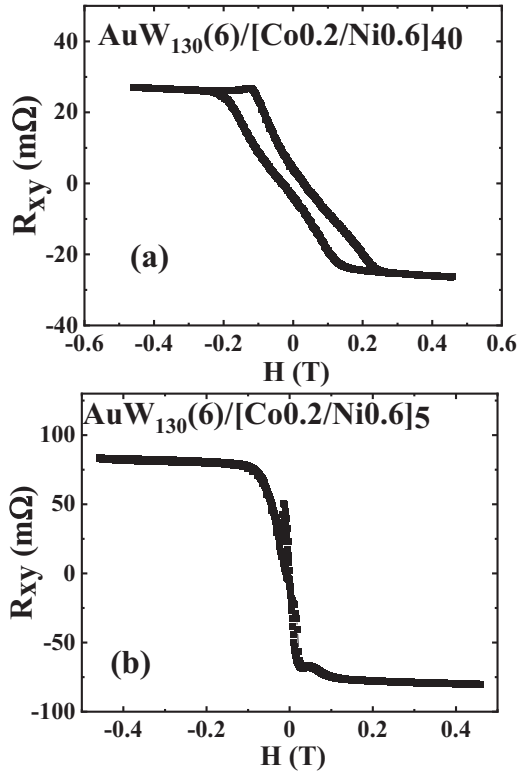


FIG. 1. Anomalous Hall effect (AHE) measurements acquired at room temperature (RT) on (a) Au : W<sub>130</sub>6nm/(Co0.2nm/Ni0.6nm)<sub>40</sub> and (b) Au : W<sub>130</sub>6nm/(Co0.2nm/Ni0.6nm)<sub>5</sub> ML samples showing the conventional negative AHE sign for the Co0.2/Ni0.6 multilayers. Samples are of type II and characterized by a large Au:W resistivity ( $\rho \simeq 130 \mu\Omega \text{ cm}$ ).

respectively, to  $N = 3, 4, 5, 6, 7$ , and 20. It is now quite remarkable that the AHE for the type-II Pt-based buffer becomes positive for  $N = 3-7$ , which is of the opposite sign compared to the Au:W type-I reference sample series described above. In that sense, such sign inversion constitutes a major AHE property identified in the present investigation. The AHE signal, now positive, first increases in amplitude from  $\Delta R_{\text{AHE}}^{(2)} = +40 \text{ m}\Omega$  for  $N = 3$  to  $\Delta R_{\text{AHE}}^{(5)} = +60 \text{ m}\Omega$  for  $N = 5$  before decreasing for  $N = 6, 7$  to  $\Delta R_{\text{AHE}}^{(6)} = +54 \text{ m}\Omega$  and  $\Delta R_{\text{AHE}}^{(7)} = +45 \text{ m}\Omega$ , respectively. Moreover, for  $N = 20$ , the AHE becomes negative; that is, it acquires the same sign as the Au:W<sub>130</sub> reference sample with an amplitude equal to  $\Delta R_{\text{AHE}}^{(20)} = -8 \text{ m}\Omega$ . This signature of a sign change for the Pt series has to be assigned to an apparent opposite sign of the spin-orbit interactions (SOI) in Pt, at least for  $N = 3, 7$  compared to the Co/Ni and Au:W samples. Moreover, the existence of a maximum in the AHE size for  $\Delta R_{\text{AHE}}^{(5)}$  may be explained by a crossover between (i) the positive contribution of the SOI in Pt with respect to Co/Ni and (ii) the needs of a spin-polarized current provided by the Co/Ni ferromagnet MLs, as explained in Sec. IV. At this stage, two additional remarks have to be appended: (i) The sign inversion of AHE for the  $N = 3-7$  Pt series is independent of the temperature effects (not shown), as well as the sign inversion of AHE in Pt observed between  $N = 3-7$  and  $N = 20$  [90]. This makes

our results and conclusion independent of thermal effects [56]. (ii) Identical AHE experiments led with type-I (very flat) Pt samples exhibit the same trends as type II, with typical AHE sign inversion for  $N = 3-7$ . All of the experimental results concerning AHE for the three sample series (Pt and Au:W type-I and Pt type-II series) are gathered in Fig. 3.

A small OHE effect can be revealed at LT (10 K) on the different samples and all show the same OHE slope in sign with about the same amplitude corresponding to a Hall coefficient in the range  $-1, 1.5 \times 10^{-12} \text{ V cm}/(\text{A G})$ , in the exact range of what is expected from Co or Ni at RT [91]. The same sign of OHE for Co/Ni accompanied by a sign inversion for AHE represents another clear indication of the AHE reversal by proximity effects and SOI sign inversion.

Figure 3 displays both AHE resistances and effective AHE resistivities, as well as longitudinal resistivities for the whole series vs the number sequences  $N$  varying from 3 to 70. In those experiments, the structure of Co0.2/Ni0.6 bilayers is fixed, depending only on  $N$ . Figure 3(a) highlights the typical crossover from positive to negative experimental values acquired at RT, for the AHE resistance  $R_{xy}$  in the case of Pt type II. The crossover between positive to negative AHE for type II is obtained for  $N \simeq 17$ , corresponding to a total Co/Ni thickness of about 15 nm. This point indicates an exact compensation of the AHE current contribution provided by Pt (positive AHE) and Co/Ni (negative AHE) layers. On the other hand, one can observe, in the same Fig. 3(a), that the  $R_{xy}$  of the type-I Pt series follows the same features as the type-II Pt series (AHE inversion) with about equal values, before decreasing to zero and crossing to negative values for larger  $N > 70$  (the orange points and curve correspond to  $N = 70$ ). This demonstrates the strong impact of the roughness on the AHE amplitude and sign in thin multilayered samples.

Figure 3(c) gives the same plot as Fig. 3(a) in the scale of resistivity  $\rho_{xy}$  for the type-II series, whereas Fig. 3(d) displays the typical expected increase of the resistivity in the Pt type-II series from the one of pure Pt ( $17 \mu\Omega \text{ cm}$ ) to the one of Co/Ni (about  $50 \mu\Omega \text{ cm}$ ) at RT when  $N$  increases to saturate at the bulk value of Co/Ni. On the other hand, Fig. 3(b) moreover compares the AHE values obtained with both Pt and different Au:W series with Au:W<sub>130</sub> (blue triangle) and Au:W<sub>80</sub> (purple point) characterized by a lower resistivity ( $80 \mu\Omega \text{ cm}$ ) and opposite spin-Hall angle (SHA) equal to  $\theta_{\text{Au:W}_{80}} = +0.15$  [29]. The Au:W<sub>80</sub> experimental point lies between the corresponding Pt and Au:W<sub>130</sub> samples because of its intermediate SHA value between those of the two materials. One of our main conclusions is that for thin ferromagnetic stacks ( $N$  small), AHE may be strongly dependent on the heavy-metal buffer grown for PMA properties, as well as the surface roughness and, possibly, the specularly at the different interfaces of the electronic waves.

### III. MAIN PHYSICAL ISSUES OF AHE AND SHE IN TRANSITION METALS

In this section, we discuss the fundamental prerequisites for the description of (i) AHE of 3d transition metals on the basis of spin currents and spin-channel-dependent inverse SHE (ISHE) and, subsequently, (ii) ISHE in 5d transition heavy metals such as Pt or Ta. Many details can be



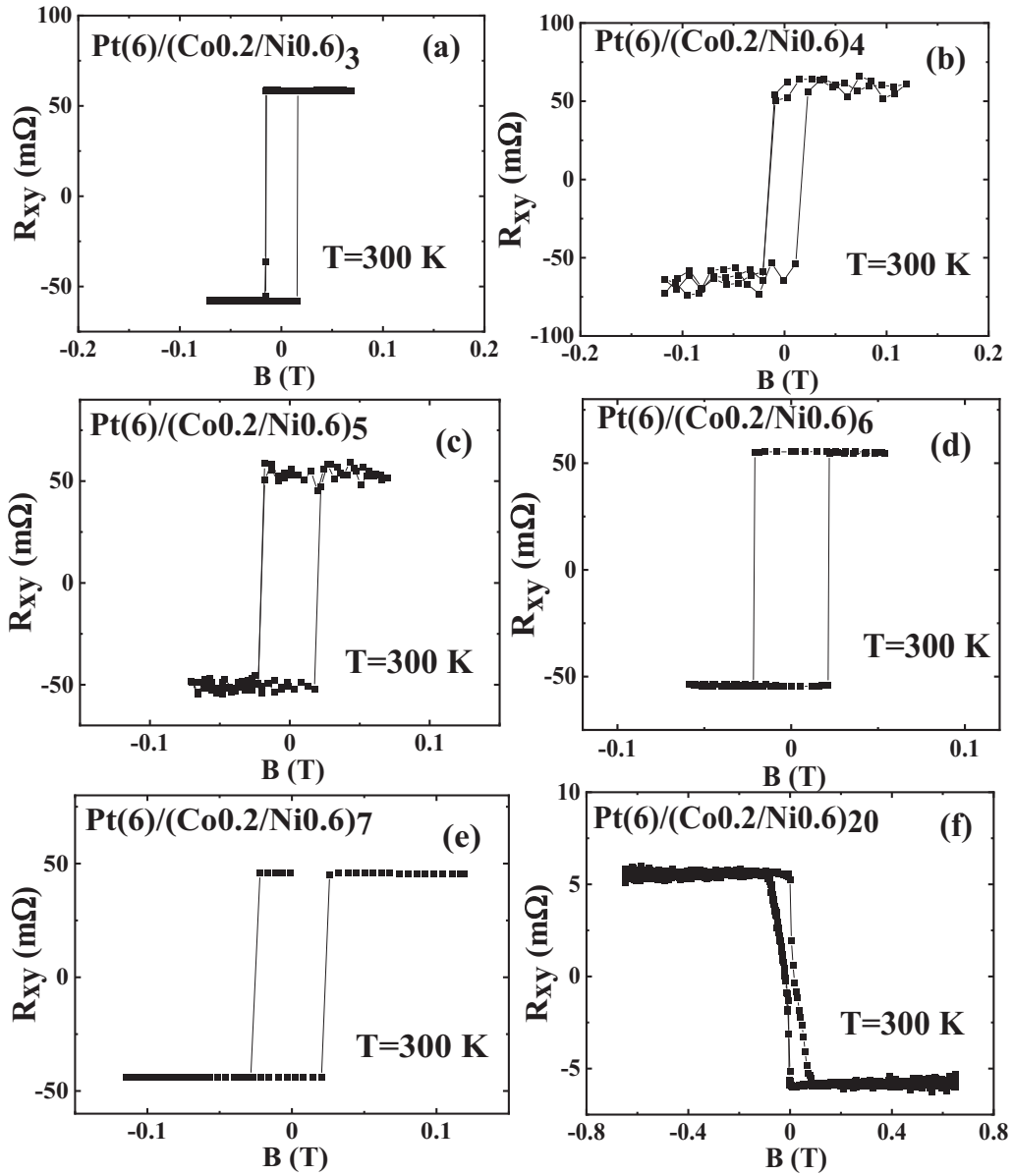


FIG. 2. Anomalous Hall effect (AHE) measurements acquired at room temperature (RT) on the type-II  $\text{Pt}6\text{nm}/(\text{Co}0.2\text{nm}/\text{Ni}0.6\text{nm})_N$  series for  $N =$  (a) 3, (b) 4, (c) 5, (d) 6, (e) 7, and (f) 20. For  $N = 3-7$ , the samples display a positive AHE, whereas for  $N = 20$ , the AHE is negative.

found in previous reference works [34–37,39,52,53,70,81], review articles [15,16], and in more recent contributive works [54–56,72,92].

### A. Linear response theory for SHE/AHE

What are the main mechanisms responsible for spin-current generation in bulk  $3d$  ferromagnets and their possible extension to spin-orbit assisted interface scattering? AHE, discovered in 1880 by Hall, precedes many of the spin-orbit effects being studied today. It describes a large magnetization-dependent Hall effect in a ferromagnetic conductor and may be decomposed into extrinsic mechanisms originating from electronic quantum diffusions and intrinsic mechanisms originating from quantum dynamics within the host material. The description of the spin-current properties and spin-dependent

conduction or conductivity may be, at a first stage, handled via a  $2 \times 2$  band model within the linear response theory adapted from Kubo's approach. The system accounts for a Hamiltonian of the type

$$\hat{H} = \frac{\hbar^2 \hat{\mathbf{p}}^2}{2m^*} + \hat{V}(\mathbf{r}) + \frac{\lambda_{\text{SO}}}{\hbar} (\hat{\nabla} \hat{V}(\mathbf{r}) \times \hat{\mathbf{p}}) \cdot \hat{\sigma}, \quad (2)$$

written in a two-band spinor form and where  $\mathbf{k}$  is the electronic wave vector,  $\hat{V}(\mathbf{r})$  is the local spherical energy potential experimented by the  $sp$ - $d$  electron ( $\hat{V}$  stands then for the potential energy  $eV$  for the sake of simplicity), and  $\lambda_{\text{SO}}$  is the spin-orbit strength in units of a (spin-orbit) cross section or area. Inside  $V(\mathbf{r})$ , the external electron potential responsible for the electron drift induced by the external electric field  $\mathbf{E}$  is also included. Moreover, inside  $\lambda_{\text{SO}} \hat{\sigma} \cdot [\hat{\mathbf{p}} \times \nabla eV(\mathbf{r})]$ , the Rashba Hamiltonian arising from the action of  $\mathbf{E}$  at

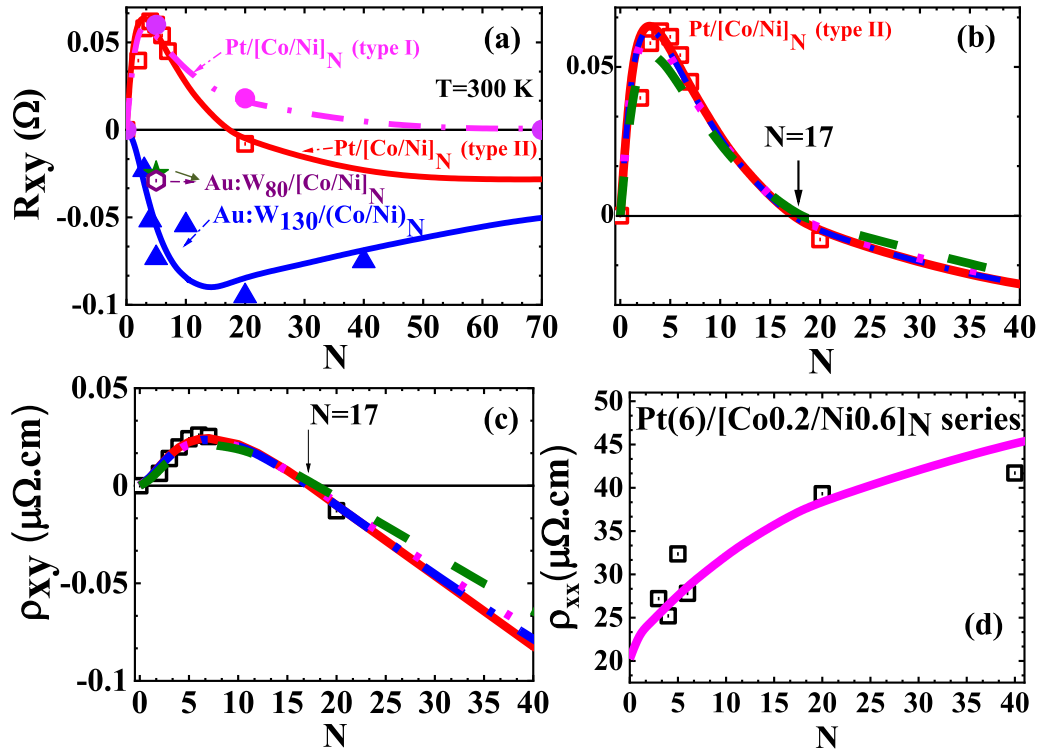


FIG. 3. (a) AHE resistance and resistivity vs the number of sequence  $N$  of Co/Ni for (a) the Pt type-I (magenta dots) and type-II (red squares) series. The AHE resistance for the Au:W<sub>130</sub> series (blue triangle) and Au:W<sub>80</sub> (purple point and green star) compared to Pt is also reported. (b) Different fits for the type-II Pt series are represented in lines corresponding to intrinsic AHE in Co/Ni (red straight line) or different models for extrinsic SHE (blue dashed line, purple point line, and green short dashed line); refer to Sec. IV for the discussion. (c) The corresponding AHE resistivities  $\rho_{xy}$  vs  $N$  for type-II Pt (black squares). (d) Longitudinal resistivities of Pt type-II samples vs  $N$  compared to the resulting fit (red line). The ensemble of parameters used for the fit of type-II Pt is gathered in Table I.

interfaces on the electronic band structure may be included. We note, respectively,  $|\mathbf{k}, n, s\rangle$  and  $|\mathbf{k}', m, s'\rangle$  (with  $\mathbf{p} = \hbar\mathbf{k}$ ), with the respective ingoing and outgoing electronic states diffused away from a scattering center and acting as a local spin-orbit perturbation  $\delta\hat{V}(\mathbf{r})$  from the host. Here,  $n$  and  $m$  are the band index, whereas  $s = \uparrow, \downarrow$ , and we note that  $s' = \uparrow, \downarrow$  is the spin index.

The anomalous Hall conductivity (AHC) for transition-metal ferromagnets may be derived from the sum of the spin-selected conductivities, whereas the spin-Hall conductivity (SHC) derives from its difference. The selected spin conductivity  $\sigma_{xy}^s$  then may be written as

$$\sigma_{xy}^s = \frac{\sigma_{xy}^{\text{AHE}} \pm \sigma_{xy}^{\text{SHE}}}{2}, \quad (3)$$

with the  $+$  ( $-$ ) sign corresponding to the spin  $\uparrow$  (spin  $\downarrow$ ). One must be careful with the particular geometry configuration of a magnetization aligned along the normal direction to the layer ( $z$ ). When the magnetization is rotated away from the  $z$  direction, other types of spin current, expressed in a vectorial form, may appear as the spin anomalous Hall effect (SAHE) [59,60].

Within the linear response theory, the Kubo formalism relates both the conductivity and the spin conductivity to the equilibrium current-current and spin-current correlation functions. This technique provides a fully quantum mechanical, formally exact expression for the conductivity within the

linear response theory [72]. We emphasize the key issues in investigating the AHE/SHE properties within this formalism in order to adapt it for the case of multilayered systems. For the purpose of studying the AHE/SHE, it is worthwhile to formulate the current-current and the spin current-current correlation within the Kubo formula in the form of the so-called Kubo-Bastin formula. If one denotes  $\hat{v}_\alpha = \frac{p_\alpha}{m^*}$  as the velocity along  $\alpha$ , and  $\{\hat{v}_\beta\sigma^\gamma\} = \frac{\hat{v}_\beta\sigma^\gamma + \sigma^\gamma\hat{v}_\beta}{2}$  the spin current flowing along the  $\beta$  direction with spin directed along the  $\gamma$  axis in a symmetrized form ( $\sigma^0 = \hat{I}$  the unit matrix for the charge conductivity), then the Kubo-Bastin formula reads

$$\sigma_{\alpha\beta}^\gamma = -\frac{e^2\hbar}{2\pi\mathcal{V}} \int f(\varepsilon) \text{Tr} \left\langle \hat{v}_\alpha \frac{\partial G^R(\varepsilon)}{\partial \varepsilon} \{\hat{v}_\beta \sigma^\gamma\} [G^R(\varepsilon) - G^A(\varepsilon)] - \hat{v}_\alpha [G^R(\varepsilon) - G^A(\varepsilon)] \{\hat{v}_\beta \sigma^\gamma\} \frac{\partial G^A(\varepsilon_F)}{\partial \varepsilon} \right\rangle > d\varepsilon,$$

where  $G^{R,A} = \frac{1}{\varepsilon - \hat{H} \pm i\Gamma}$  is the respective retarded (R) and advanced (A) Green's function, with  $\varepsilon$  the energy,  $\Gamma$  the energy broadening,  $f(\varepsilon)$  the Fermi occupation function, and Tr the trace over  $\mathbf{k}$  and band index  $n$ . By integration of the previous integral by parts, the spin conductivity breaks up into  $\sigma_{\alpha\beta}^\gamma = \sigma_{\alpha\beta}^{\gamma,I} + \sigma_{\alpha\beta}^{\gamma,II}$ , where  $\sigma_{\alpha\beta}^{\gamma,I}$  and  $\sigma_{\alpha\beta}^{\gamma,II}$  stand, respectively, for the Fermi surface (spin-conductivity) term and  $\sigma_{\alpha\beta}^{\gamma,II}$  for

the Fermi sea (spin-conductivity) term according to

$$\sigma_{\alpha\beta}^{\gamma,I} = \frac{e^2\hbar}{2\pi\mathcal{V}} \text{Tr}\langle \hat{v}_\alpha G^R(\varepsilon_F) \{ \hat{v}_\beta \sigma^\gamma \} G^A(\varepsilon_F) \rangle - \frac{1}{2} \langle R \rightarrow A + A \rightarrow R \rangle$$

and

$$\sigma_{\alpha\beta}^{\gamma,II} = \frac{e^2\hbar}{4\pi\mathcal{V}} \int d\varepsilon f(\varepsilon) \text{Tr} \left\langle \hat{v}_\alpha G^R(\varepsilon) \{ \hat{v}_\beta \sigma^\gamma \} \frac{\partial G^R(\varepsilon)}{\partial \varepsilon} - \hat{v}_\alpha \frac{\partial G^R(\varepsilon)}{\partial \varepsilon} \{ \hat{v}_\beta \sigma^\gamma \} G^R(\varepsilon) + \text{c.c.} \right\rangle.$$

SHC and AHC originate from the same general formula that is representative of the linear response theory. The difference lies in that the formula involves a symmetrization ({} procedure because it involves noncommutative Pauli matrices for the spin. In that sense, both quantities, SHE and AHE, are connected to each other.

We are going to describe the different contributions to the spin current or spin-Hall conductivities (SHCs) in terms of the *extrinsic vs intrinsic* effect. Kontani *et al.* [70] and Tanaka *et al.* [52] conclude that the origin of SHC in transition metals, i.e., 3d ferromagnet or 5d heavy metals, depends on the degree of disorder and on the characteristic energy broadening ( $\Gamma$ ). At small disorder (small  $\Gamma$ ), SHC is intrinsic and originates mainly from the contribution of the Fermi sea term  $\sigma_{xy}^{II}$  (interband contribution). On the other hand, as the disorder increases (large  $\Gamma$ ), the Fermi surface term (intra-band contribution) becomes dominant.

### 1. Intrinsic AHE/SHE

The intrinsic spin conductivity mainly originates from the Fermi sea terms and it can be derived from the expansion of the Kubo-Bastin formula (4) for the host. It is written in the general case as

$$\sigma_{\alpha\beta}^{\gamma} = 2 \frac{e^2\hbar}{\mathcal{V}} \text{Im} \sum_{kn,km} [f(\varepsilon_n) - f(\varepsilon_m)] \times \frac{\langle kn | \{ \hat{\sigma}^\gamma \hat{v}_\alpha \} | km \rangle \langle km | \hat{v}_\beta | kn \rangle}{(\varepsilon_{nk} - \varepsilon_{mk})^2},$$

where  $f$  is the Fermi occupation function,  $|n\rangle$  and  $|m\rangle$  are, respectively, the *occupied* and *unoccupied* electronic state,  $\varepsilon_{km} - \varepsilon_{kn}$  is the corresponding excitation energy,  $\hat{v}$  is the velocity operator,  $\hat{\sigma}$  is the Pauli matrix,  $\alpha, \beta$  are two indices for the space coordinates,  $xx$  and  $xy$  are the respective longitudinal and transverse spin Hall conductivity, and  $\text{Im}$  is the imaginary part. When  $\gamma = z$  defines the spin direction along  $z$ , it leads, *in fine*, to [53]

$$\sigma_{xy}^z = 2 \frac{e^2\hbar}{\mathcal{V}} \text{Im} \sum_n f(\varepsilon_n) \Omega_{(n)}^z,$$

where  $\Omega_{(n)}^z = \text{Im} \sum_{km \neq n} \frac{\langle kn | \{ \hat{\sigma}^z \hat{v}_x \} | km \rangle \langle km | \hat{v}_y | kn \rangle}{(\varepsilon_{kn} - \varepsilon_{km})^2}$  stands for the Berry curvature corresponding to band  $n$ .

### 2. Extrinsic skew-scattering AHE/SHE

We are now going to describe AHE/SHE in the limit of strong scattering. Smit [35,36] proposed the skew-scattering mechanism as the source of the AHE. Indeed, in the presence of spin-orbit interactions (SOI), the matrix element of the impurity scattering potential reads

$$\langle \mathbf{k}' s' | \delta \hat{V} | \mathbf{k} s \rangle = \tilde{V}_{\mathbf{k},\mathbf{k}'} [\delta_{s,s'} + \lambda_{\text{SO}} \langle s' | \hat{\sigma} | s \rangle \cdot (\mathbf{k}' \times \mathbf{k})] \quad (4)$$

for a spherical perturbation  $\delta \hat{V}$ . A microscopic detailed balance would require that the transition probability  $W_{n \rightarrow m}$  between states  $|k, n, s\rangle$  and  $|k', m, s\rangle$  be identical, at a second order of perturbation, to that proceeding in the opposite direction  $W_{m \rightarrow n}^{(2)}$ . It holds for the Fermi's golden-rule approximation,

$$W_{k \rightarrow k'} = \frac{2\pi}{\hbar} |\langle \mathbf{k}' s' | \delta \hat{V} | \mathbf{k} s \rangle|^2 \delta(\varepsilon_{k'n} - \varepsilon_{k's}). \quad (5)$$

At higher order, the transition rate  $W_{\mathbf{k}\mathbf{k}'}$  is given by the  $T$ -matrix element of the disorder potential,  $W_{\mathbf{k}\mathbf{k}'} \simeq \frac{2\pi}{\hbar} |T_{\mathbf{k}\mathbf{k}'}|^2 \delta(\varepsilon_{k'} - \varepsilon_k)$ . The scattering  $T$  matrix is more generally defined as  $T_{\mathbf{k}\mathbf{q}'} = \langle \mathbf{q}' | \delta \hat{V} | \mathbf{k} \rangle$ , with  $\mathbf{q}$  being the eigenstate of the full Hamiltonian involving the perturbation  $\delta \hat{V}$ . For a weak disorder, one can approximate the scattering state  $|\mathbf{q}'\rangle$  by a truncated series in powers of  $\delta V_{\mathbf{k}\mathbf{k}'}$  according to

$$|\mathbf{q}\rangle = |\mathbf{k}\rangle + \sum_{\mathbf{k}''} \frac{\delta V_{\mathbf{k}''\mathbf{k}}}{\varepsilon_{\mathbf{k}} - \varepsilon_{\mathbf{k}''} + i\eta} |\mathbf{k}''\rangle. \quad (6)$$

Using this expression in the above definition of the  $T$  matrix, one can expand the scattering rate in powers of the disorder strength up to the order two (leading to no scattering asymmetry terms) or up to the order three (leading to scattering asymmetry terms) giving, *in fine*,

$$W_{\mathbf{k}\mathbf{k}'}^{(3)} = \frac{2\pi}{\hbar} \left( \sum_{\mathbf{k}''} \frac{\langle \delta \hat{V}_{\mathbf{k}'\mathbf{k}''} \delta \hat{V}_{\mathbf{k}''\mathbf{k}} \delta \hat{V}_{\mathbf{k}\mathbf{k}'} \rangle}{\varepsilon_{\mathbf{k}} - \varepsilon_{\mathbf{k}''} + i\eta} + \text{c.c.} \right) \delta(\varepsilon_{\mathbf{k}} - \varepsilon_{\mathbf{k}'}), \quad (7)$$

which yields, *in fine*,

$$W_{\mathbf{k}\mathbf{k}'}^{(3)} = - \frac{(2\pi)^2}{\hbar} \lambda_{\text{SO}} \mathcal{N}(\varepsilon_F) \hat{V}^3 (\mathbf{k}' \times \mathbf{k}) \cdot \hat{\sigma} \delta(\varepsilon_{\mathbf{k}} - \varepsilon_{\mathbf{k}'}) \delta_{\sigma\sigma'} \quad (8)$$

for the asymmetry term we are searching for ( $\text{Im}$  is the imaginary part), and  $\mathcal{N}(\varepsilon_F)$  is the density of states at the Fermi level. In the calculations of the Hall conductivity, which involve the second Born approximation (third order in  $V$ ), detailed balance already fails. In the case of  $p$  orbitals, skew scattering can be represented by an asymmetric part of the transition probability,

$$W_{\mathbf{k}\mathbf{k}'}^A = -\tau_A^{-1} (\mathbf{k} \times \mathbf{k}') \cdot \hat{\mathbf{m}}. \quad (9)$$

When the asymmetric scattering processes are included (called skew scattering), the scattering probability  $W_{\mathbf{k}\mathbf{k}'}$  is distinct from  $W_{\mathbf{k}'\mathbf{k}}$ . Physically, scattering of a carrier from an impurity introduces a momentum perpendicular to both the incident momentum  $k$  and the magnetization  $\mathbf{m}$ . This leads to a transverse current proportional to the longitudinal current driven by the electric field  $\mathbf{E}$ .

### 3. Extrinsic side-jump AHE and SHE

The side-jump mechanism mainly originates from the Fermi surface term. The basic semiclassical argument is the

following: when considering the scattering of a Gaussian wave packet from a spherical impurity with SOI (with  $H_{\text{SO}} = \lambda_{\text{SO}} L_z S_z$ ), a wave packet with an incident wave vector  $\mathbf{k}$  will experiment a displacement transverse to  $\mathbf{k}$  and  $\mathbf{E}$ . This type of contribution was first noticed, but discarded, by Smit [36] and reintroduced afterwards by Berger, who argued that it was the main contribution to the AHE. The derivation of the side-jump process can be made by the following semiphenomenological arguments. The change in the velocity during the diffusion process by a central potential  $\delta\hat{V}(r)$  is simply

$$\hat{\mathbf{v}}_i = \frac{\partial \hat{\mathbf{r}}_i}{\partial t} = \frac{1}{i\hbar} [\hat{\mathbf{r}}_i, \hat{H}] = \frac{\hat{\mathbf{p}}_i}{m^*} - \frac{\lambda_{\text{SO}}}{\hbar} [\nabla \delta\hat{V}(r) \times \hat{\sigma}]. \quad (10)$$

However, the dynamics of the electron is also described by

$$\frac{\partial \hat{\mathbf{p}}_i}{\partial t} = \frac{1}{i\hbar} [\hat{\mathbf{p}}_i, \hat{H}] \simeq -\nabla \delta\hat{V}(r), \quad (11)$$

and we get the anomalous Hall velocity:

$$\hat{\mathbf{v}}_i = \frac{\hat{\mathbf{p}}_i}{m} + \frac{\lambda_{\text{SO}}}{\hbar} \left( \frac{\partial \hat{\mathbf{p}}}{\partial t} \times \hat{\sigma} \right)_i. \quad (12)$$

The time integration of the last quantity gives the lateral shift coordinate  $\Delta \mathbf{r}_i$  (here,  $i$  represents the transverse direction) experienced by a carrier during a scattering event,

$$\Delta \mathbf{r}_i = \frac{\lambda_{\text{SO}}}{\hbar} (\Delta \mathbf{p} \times \hat{\sigma})_i, \quad (13)$$

and the transverse side-jump velocity  $\mathbf{v}_{sj}$  results in

$$\mathbf{v}_{sj} = \frac{\lambda_{\text{SO}}}{\hbar} \frac{\Delta \mathbf{p} \times \hat{\sigma}}{\tau_p}, \quad (14)$$

where  $\tau_p$  is the characteristic momentum scattering time and  $\Delta \mathbf{p} = e\mathbf{E}\tau_p$  is the change of the particle impulsion after its isotropic diffusion. We get the side-jump current along the direction normal to both electric field  $\mathbf{E}$  and spin direction  $\sigma$  according to

$$\mathbf{j}^{sj} = \frac{ne^2\lambda_{\text{SO}}}{\hbar} (\mathbf{E} \times \hat{\sigma}), \quad (15)$$

and where  $n$  is the density of carriers. Note that the side-jump mechanism, like the intrinsic AHE and SHE, is independent of the scattering time. A detailed expression of the anomalous Hall velocity in a multiband picture for TM have been derived by Levy [93] using phase-shift analyses.

### B. Model for AHE and SHE for 3d ferromagnets and 5d heavy metals

From the fundamental principle described above, we now turn to the description of spin-Hall effects (SHE) and the anomalous Hall effect in transition-metal 3d ferromagnets. This connection is described by the off-diagonal terms of conductivity tensors  $\sigma_{xy}$  for a spin direction aligned along  $\hat{z}$ : whereas SHE is described via the spin-dependent ( $\uparrow, \downarrow$  spins) conductivity tensors, the AHE considers the sum of those two spin-dependent contributions according to

$$\hat{\sigma}_{\alpha\beta} = \hat{\sigma}_{\alpha\beta}^{\uparrow} + \hat{\sigma}_{\alpha\beta}^{\downarrow} = \begin{pmatrix} \sigma_{xx}^{\uparrow} + \sigma_{xx}^{\downarrow} & \sigma_{xy}^{\uparrow} + \sigma_{xy}^{\downarrow} \\ -(\sigma_{xy}^{\uparrow} + \sigma_{xy}^{\downarrow}) & \sigma_{xx}^{\uparrow} + \sigma_{xx}^{\downarrow} \end{pmatrix}, \quad (16)$$

where  $\sigma_{xx}^{\uparrow, \downarrow}$  represents the longitudinal conductance along the electric-field direction ( $x$ ), and  $\sigma_{xy}^{\uparrow, \downarrow}$  is the off-diagonal or

transverse part responsible for both SHE and AHE phenomena with transverse particle flow along  $y$ . Accordingly, SHE and AHE are both described by their own angle related by

$$\theta_{SHE}^s = \frac{\sigma_{xy}^s}{\sigma_{xx}^s}, \quad \theta_{AHE} = \frac{\sigma_{xy}^{\uparrow} + \sigma_{xy}^{\downarrow}}{\sigma_{xx}^{\uparrow} + \sigma_{xx}^{\downarrow}}. \quad (17)$$

For ferromagnetic materials such as Co, Ni, or Co/Ni,  $\theta^{\downarrow}$  differs from  $\theta^{\uparrow}$  due to the lift in the energy spin degeneracy, particularly at the Fermi level [94], whereas for nonmagnetic materials, such as Pt, one has  $\theta^{\downarrow} = -\theta^{\uparrow}$  by simple symmetry arguments. The last expression for the AHE angle gives the correspondence between the respective AHE and SHE mechanisms. The spin-dependent conductivity and resistivity tensors are inverse to each others. One considers the respective off-diagonal components, which mainly are written as a sum of three different physical contributions, i.e., *extrinsic* skew scattering (*sk*), *extrinsic* side-jump (*sj*), and *intrinsic* (*int*) parts [15,16,73], as  $\sigma_{xy}^s = \theta^{sk,s} \sigma_{xx}^s + \sigma_{xy}^{sj,s} + \sigma_{xy}^{int,s}$ , giving thus the expression of the AHE in the conductivity tensor by summing the two spin-channel contributions  $\sigma_{xy} = \theta^{sk} \sigma_{xx} + \sigma_{xy}^{sj} + \sigma_{xy}^{int}$  with  $\theta^{sk} = \frac{\theta^{sk,\uparrow} \sigma_{xx}^{\uparrow} + \theta^{sk,\downarrow} \sigma_{xx}^{\downarrow}}{\sigma_{xx}^{\uparrow} + \sigma_{xx}^{\downarrow}}$ ,  $\sigma_{xy}^{sj} = \sigma_{xy}^{sj,\uparrow} + \sigma_{xy}^{sj,\downarrow}$ , and  $\sigma_{xy}^{int} = \sigma_{xy}^{int,\uparrow} + \sigma_{xy}^{int,\downarrow}$ . The rule to sum the different contributions to the off-diagonal transverse components for the conductivity tensors, i.e., for different series processes in the electronic transport, originates from the same form of the off-diagonal components of the resistivity tensor,

$$-\rho_{xy}^s = \theta^{sk,s} \rho_{xx}^s + (\sigma_{xy}^{sj,s} + \sigma_{xy}^{int,s}) (\rho_{xx}^{s2} + \rho_{xy}^{s2}), \quad (18)$$

where  $\theta^{sk,\uparrow,\downarrow}$ ,  $\sigma_{xy}^{sj,\uparrow,\downarrow}$ , and  $\sigma_{xy}^{int,\uparrow,\downarrow}$  may be considered as independent of the resistivity of the host material, which makes such formula very general and useful in practical cases [56]. If one considers only extrinsic skew-scattering SHE/AHE processes [39], one finally gets  $\rho_{AHE} = -(\rho_{xy}^{\uparrow} \frac{\rho_{xx}^2}{\rho_{xx}^2} + \rho_{xy}^{\downarrow} \frac{\rho_{xx}^2}{\rho_{xx}^2})$  like proposed in Ref. [95], giving, *in fine* [39],

$$-\rho_{AHE} = \left( \frac{\rho_{xy}^{\uparrow} + \rho_{xy}^{\downarrow}}{4} \right) [1 + \mathcal{P}^2(z)] + \left( \frac{\rho_{xy}^{\uparrow} - \rho_{xy}^{\downarrow}}{2} \right) \mathcal{P}, \quad (19)$$

with the local spin polarization  $\mathcal{P}(z)$  within the multilayer along the coordinate  $z$ .  $\mathcal{P}(z) = \frac{\sigma_{xx}^{\uparrow}(z) - \sigma_{xx}^{\downarrow}(z)}{\sigma_{xx}^{\uparrow}(z) + \sigma_{xx}^{\downarrow}(z)}$  is the spin polarization  $\mathcal{P}(z)$  that we have to calculate with our numerical procedure. The partition of the AHE resistivity according to the formula [19] was discussed by Fert *et al.* as the partition between the *spin effect* (first term on the right-hand side) and the *pure skew-scattering effect* (second term on the right-hand side). Such partition is also discussed in term of the *SAHE* (spin anomalous Hall effect) and *SHE* for a magnetization control of the spin currents in ferromagnets [59]. This second term (SHE) is also present for nonmagnetic materials, giving rise to the standard SHE as far as  $\rho_{xy}^{\downarrow} - \rho_{xy}^{\uparrow}$  when the time-reversal symmetry may act (no magnetism).

### C. AHE in multilayers

Our analyses are based on a semiphenomenological approach of spin-dependent transport, involving spin-dependent diffusion and electron scattering at the multiple interfaces, possibly considering spin flips caused by the local spin-orbit interactions. The principle of the method is then as follows:



(1) A representation of the spin-current profiles within the multilayer by correctly matching the out-of-equilibrium electronic Fermi distributions. This is of primary importance to provide the amplitude of the anomalous Hall effect (AHE) in multilayers as far as a ferromagnetic layer ensures the polarization of the current via the nonlocal spin-dependent conductivity calculated by this method.

(2) the adjacent layer (Pt, Au:W) of a large spin-orbit coupling (SOC) can affect the spin-orbit assisted diffusion of electrons by the *spin-current proximity effect*. Therefore, the AHE may be enhanced by increasing the spin-orbit coupling in the SOC layer. The more important is the SOC, the larger is the transverse spin current via the spin-to-charge conversion process and the anomalous Hall angle. However, AHE may invert its sign by changing the sign of the SOC (Pt/CoNi, even Au:W<sub>80</sub>).

In the case of multilayers, nonlocal spin-dependent conductivities are necessary to consider, leading to important spin-current proximity effects. Consequently, the theory beyond a standard linear theory response of bulk materials as described here is necessary to correctly interpret the data. Our semiphenomenological approach of spin-orbit polarized transport in magnetic multilayers, presented here, is based on a generalization of the theory of Camley-Barnas [85,86,96]. The counterpart of the relative simplicity of such semiclassical modeling is to find the appropriate boundary conditions to be adopted at interfaces such as the ones proposed in Ref. [87]. Those are given by a certain continuity/discontinuity relation of the out-of-equilibrium distributions of the functions of the Fermi surface vs the transmission or reflection coefficients of the electronic waves and another coefficient of specularity  $p$ . This coefficient of specularity  $p$  reflects the effects of “isotropic” diffusions on the impurities at the interfaces and therefore plays a major role in particular on the properties of electronic reflection. Adapting the Camley-Barnas model to the model of Kubo-Greenwood’s linear response in multilayers therefore requires finding the correct semiphenomenological parameter set at the interfaces in order to fairly describe the diffusion properties.

### 1. General overview

In the current-in-plane (CIP) geometry, spin-polarized currents are translationally invariant along the flow direction, leading to a divergent current by construction with the results that no charge or spin accumulation occurs. The only first term to consider is the displacement of the spin-polarized currents on the Fermi surface. The counterpart for CIP currents is that one cannot define a single out-of-equilibrium length of the Fermi distribution near each interface, being scaled for each direction by a  $\cos(\theta)$  feature where  $\theta$  represents the angle of incidence with respect to the multilayered surface. In a semiclassical approach, CIP can be described through the well-parametrized Boltzmann theory adapted to spin-polarized transport according to the following general equation applied to the out-of-equilibrium Fermi distribution  $f_s(\mathbf{r}, \mathbf{v}, \mathbf{E}, t)$  of spin  $s$  under the application of an electric field  $\mathbf{E}$  along the  $z$  direction perpendicular to the layers according to

$$f^s(z, \mathbf{v}) = f_0(\mathbf{v}) + g^s(z, \mathbf{v}), \quad (20)$$

where we note that  $e = |e|$  is the absolute value of the electron charge,  $\mathbf{v}$  is the electron velocity, and where the distribution function for the electron is decomposed into two parts: the equilibrium in the zero electric-field distribution function  $f_0(\mathbf{v})$  and a small perturbation  $g^s(z, \mathbf{v})$  induced by the electric field and the interface scattering perturbation. The general solution  $g^s(z, \mathbf{v})$  in each layer now reads

$$g^s(z, \mathbf{v}) = \begin{cases} \frac{eE\tau^s}{m} \frac{\partial f_0(\mathbf{v})}{\partial v_x} \left[ 1 + F_+^s(\mathbf{v}) \exp\left(\frac{-z}{\tau^s |v_z|}\right) \right] & \text{for } v_z > 0 \\ \frac{eE\tau^s}{m} \frac{\partial f_0(\mathbf{v})}{\partial v_x} \left[ 1 + F_-^s(\mathbf{v}) \exp\left(\frac{z}{\tau^s |v_z|}\right) \right] & \text{for } v_z < 0, \end{cases} \quad (21)$$

where  $F_{\pm}^s(\mathbf{v})$  are arbitrary functions of the electron velocity and found by the matching conditions. The current density for the spin  $s$  is given by

$$J^s(z) = -2|e| \left(\frac{m}{\hbar}\right)^3 \int_V v_x g_x^s(z, \mathbf{v}) d\mathbf{v}, \quad (22)$$

where  $V$  is the unit volume,  $d\mathbf{v} = dv_x dv_y dv_z$  represent the three-dimensional (3D) velocity space, and  $g^s(z, \mathbf{v})$  may be decomposed into a bulk term  $g_0^s$ , plus an out-of-equilibrium interface term  $\delta g^s$  and originating from interface scattering with the result that  $g^s = g_0^s + \delta g^s$ .

### 2. Treatment in multilayers

All of the matching conditions for the out-of-equilibrium Fermi distribution  $g^s$  to fulfill at the interfaces are considered via the  $S$ -scattering matrix formalism.  $g_0^s$  and  $\delta g^s$  describe, respectively, the bulk conduction and the perturbation originating from the interface terms due to interface scattering (reflection/transmission). In a spinor form, we have  $g_0 = [g_0^\uparrow, g_0^\downarrow]^T$  and  $\delta g_0 = [\delta g_0^\uparrow, \delta g_0^\downarrow]^T$ , to give  $g = [g^\uparrow, g^\downarrow]^T = [g_0^\uparrow + \delta g_0^\uparrow, g_0^\downarrow + \delta g_0^\downarrow]^T$ , where  $g^+$  is for electrons possessing a positive velocity  $v_z$  along  $z$ , and  $g^-$  is for carriers with opposite velocity  $-v_z$ .

If one considers the scattering at a single interface and before generalizing to multilayers, it may be written as

$$\begin{pmatrix} g_L^- \\ g_R^+ \end{pmatrix} = \begin{pmatrix} R & T' \\ T & R' \end{pmatrix} \begin{pmatrix} g_L^+ \\ g_R^- \end{pmatrix}, \quad (23)$$

where  $g_L^\pm$  and  $g_R^\pm$  represent the respective distribution functions to the left and to the right of the interface;  $T, R$  are the respective transmission and reflection spin-dependent transmission coefficients from the left to the right; and whereas  $T', R'$  are those from the right to the left. The transmission and reflection coefficients are built in a  $2 \times 2$  matrix form, with e.g.,  $R = \begin{pmatrix} R^{\uparrow\uparrow} & R^{\uparrow\downarrow} \\ R^{\downarrow\uparrow} & R^{\downarrow\downarrow} \end{pmatrix}$  and  $T = \begin{pmatrix} T^{\uparrow\uparrow} & T^{\uparrow\downarrow} \\ T^{\downarrow\uparrow} & T^{\downarrow\downarrow} \end{pmatrix}$ , where the respective  $\uparrow\uparrow$  and  $\downarrow\downarrow$  stand for the spin-conserving terms, whereas  $\uparrow\downarrow$  and  $\downarrow\uparrow$  stand for the spin-flip terms. Therefore,

$$T = \begin{bmatrix} T^\uparrow \left(1 - \frac{sf}{2}\right)^2 + T^\downarrow \left(\frac{sf}{2}\right)^2 & (T^\uparrow + T^\downarrow) \frac{sf}{2} \left(1 - \frac{sf}{2}\right) \\ (T^\uparrow + T^\downarrow) \frac{sf}{2} \left(1 - \frac{sf}{2}\right) & T^\downarrow \left(1 - \frac{sf}{2}\right)^2 + T^\uparrow \left(\frac{sf}{2}\right)^2 \end{bmatrix}, \quad (24)$$

where  $T^\uparrow = \frac{T^*}{1-\gamma}$ ,  $T^\downarrow = \frac{T^*}{1+\gamma}$ , and  $T^*$  is a certain average of the transmission,  $\gamma$  is the interfacial spin-transmission asymmetry parameter,  $(sf) = 1 - \exp -\delta$  is the interfacial spin-flip probability, and  $\delta$  is the spin-memory loss parameter [97]. The same relationship exists for the reflection matrix

$R$ . The degree of specularity at the interfaces,  $sp^R$  and  $sp^T$ , in the respective reflection/transmission processes, may be taken into account via  $R = R_{sp=1} \times sp^R$  and  $T = T_{sp=1} \times sp^T$ , where  $sp = 1$  means that  $R$  and  $T$  correspond to full specular processes.

### 3. The case of a single interface

The case of a single interface is then treated by the following relationship, linking the left and right out-of-equilibrium components:

$$\begin{pmatrix} 1_{2 \times 1} \\ \delta g_L^- \\ \delta g_R^+ \end{pmatrix} = \begin{pmatrix} 1_{2 \times 2} & 0_{2 \times 2} & 0_{2 \times 2} \\ \Sigma^{(+)} & R & T' \\ \Sigma^{(-)} & T & R' \end{pmatrix} \begin{pmatrix} 1_{2 \times 1} \\ \delta g_L^+ \\ \delta g_R^- \end{pmatrix}, \quad (25)$$

where  $1_{2 \times 1} = \begin{pmatrix} 1 \\ 1 \end{pmatrix}$ ,  $1_{2 \times 2} = \begin{pmatrix} 1 & 0 \\ 0 & 1 \end{pmatrix}$ , and  $0_{2 \times 2} = \begin{pmatrix} 0 & 0 \\ 0 & 0 \end{pmatrix}$ , with the source terms  $\Sigma^{(+)}$  and  $\Sigma^{(-)}$  written in a  $2 \times 2$  diagonal matrix form:

$$\Sigma^{(+)} = [(R - 1)g_{0L} + T'g_{0R}], \quad (26)$$

$$\Sigma^{(-)} = [Tg_{0L} + (R' - 1)g_{0R}], \quad (27)$$

where we have considered the respective *left-traveling* ( $-$ ) and *right-traveling* ( $+$ ) electrons and their bulk out-of-equilibrium Fermi distributions,  $g_{0L}^+ = g_{0L}^- = g_{0L}$  and  $g_{0R}^+ = g_{0R}^- = g_{0R}$ , at the respective left ( $L$ ) and right ( $R$ ) side of the interface. The following  $S_{6 \times 6}$  matrix is revealed to be the relevant scattering matrix to find the interfacial out-of-equilibrium distribution function:

$$S = \begin{pmatrix} 1_{2 \times 2} & 0_{2 \times 2} & 0_{2 \times 2} \\ \Sigma^{(+)} & R & T' \\ \Sigma^{(-)} & T & R' \end{pmatrix}, \quad (28)$$

before generating it by recursion to the case of multiple interfaces.

### 4. Case of multiple interfaces: The scattering-path method

One has to define here each propagation matrix  $P^{(i)}$  inside a given layer  $i$  as  $P^{(i)} = \text{Diag}_{2 \times 2}[\exp\{-\frac{d^{(i)}}{\lambda^{(\uparrow)} \cos \theta}\}; \exp\{-\frac{d^{(i)}}{\lambda^{(\downarrow)} \cos \theta}\}]$ , where  $d^{(i)}$  is the layer thickness of the corresponding layer and  $\lambda^{(\uparrow)(\downarrow)}$  is the mean free path of the respective  $\uparrow, \downarrow$  spin. One then uses the scattering-path method applied to the out-of-equilibrium Fermi distribution functions  $g$  to solve the entire problem. This method consists in searching for the solution of the interfacial out-of-equilibrium contribution function  $\delta g_j^\pm$  (here,  $j$  labels the interface) according to

$$\hat{g}_{\text{out}}^{(i)} = \sum_{(j)} \hat{S}^{(ij)} \hat{g}_{\text{int}}^{(j)}, \quad (29)$$

written in a supermatrix form. The ‘‘supermatrix’’ denomination means that in the above equation, we apply a double summation made on the two-dimensional spinor space (spin-conserving and spin-flip terms) as well as on the  $j$  space using twice the Einstein’s notation.  $\hat{S}$  is a  $6N \times 6N$  matrix size, with  $N$  the number of interfaces. It has the meaning of finding the correlation between the transmitted and reflected out-of-equilibrium function distribution at the surface  $i$  from

*perturbations* generated from the interface  $j$ , and where

$$\hat{g}_{\text{int}} = [g_{\text{int}}^{(1)} \quad g_{\text{int}}^{(2)} \quad \dots \quad g_{\text{int}}^{(N)}]^T, \quad (30)$$

with  $g_{\text{int}}^{(N)}$  a column vector with  $g_{\text{int}}^{(1)} = (1_{2 \times 1} \quad 0_{2 \times 1} \quad \delta g_{(1)}^-)^T$ ,  $g_{\text{int}}^{(N)} = (1_{2 \times 1} \quad \delta g_{N+1}^+ \quad 0_{2 \times 1})^T$ , and  $g_{\text{int}}^{(n) \neq (1,N)} = (1_{2 \times 1} \quad 0 \quad 0)^T$  is the known  $6 \times 1$  matrix incoming or source components, whereas  $\hat{g}_{\text{out}}$  is given by

$$\hat{g}_{\text{out}}^{(i)} = [1_{2 \times 1} \quad \delta g_{(i)}^- \quad \delta g_{(i+1)}^+]^T. \quad (31)$$

One may then consider the general relationship linking the generalized scattering matrix  $S_{nm}$  (with *large*  $S$ ) to the respective single-interface scattering matrices  $s_n$  at the interface  $n$  according to

$$S_{(ij)} = s_i \delta_{ij} - s_i P_{(il)} S_{(lj)} \quad (32)$$

or, equivalently,

$$[S]_{(ij)}^{-1} = ([s_i]^{-1} \delta_{ij} - P_{(ij)}), \quad (33)$$

where  $\delta_{ij}$  is the Kronecker symbol and where  $i, j, l$  denote the interface and  $P_{(il)}$  the propagator from the interface  $i$  to the interface  $j$ .  $s_i$  is the single-interface  $6 \times 6$  scattering matrix at the interface  $i$ . In particular, one has the self-consistent equation for each  $i$ :

$$[1_{2 \times 1} \quad \delta g_i^- \quad \delta g_{i+1}^+]^T = s_i [1_{2 \times 1} \quad \delta g_i^+ \quad \delta g_{i+1}^-]^T,$$

with

$$P_{n,n+1} = \begin{pmatrix} 0_{2 \times 2} & 0_{2 \times 2} & 0_{2 \times 2} \\ 0_{2 \times 2} & 0_{2 \times 2} & 0_{2 \times 2} \\ 0_{2 \times 2} & 1_{2 \times 2} & 0_{2 \times 2} \end{pmatrix},$$

$$P_{n+1,n} = \begin{pmatrix} 0_{2 \times 2} & 0_{2 \times 2} & 0_{2 \times 2} \\ 0_{2 \times 2} & 0_{2 \times 2} & 1_{2 \times 2} \\ 0_{2 \times 2} & 0_{2 \times 2} & 0_{2 \times 2} \end{pmatrix}, \quad (34)$$

with  $n \geq 1$ .

We have checked that our code was first able to simulate, in a very good agreement, the spin-current profiles and current-in-plane giant magnetoresistance (CIP-GMR) from Co/Cu/NiFe structures such as provided by *ab initio* techniques [87] and using known parameters for Co, Cu, and NiFe extracted from the literature [90]. Examples of calculations of the properties of a Pt/(Co,Ni) multilayered system for AHE are displayed in Fig. 4 using the ensemble of physical parameters given in Table I. Figure 4(a) displays the typical increase of the resistivity of the  $(\text{Co}_{0.2}/\text{Ni}_{0.6})_N$  system ( $N$  is the number of repetitions) from the bulk value ( $60 \mu\Omega \text{ cm}$ ) at RT up to  $110 \mu\Omega \text{ cm}$  for  $N \simeq 1-2$  due to electronic scatterings and nonspecularity at interfaces ( $sp_{\text{Co/Pt}}^R = 0$ ,  $sp_{\text{Ni/Al}}^R = 0$ , and  $sp_{\text{Co/Ni}}^R = 0.4$ ) and, in particular, at the outer boundaries of the structure. In parallel, the inset of this figure displays the dependence in  $N$  of the fraction of charge current and spin currents in Co/Ni. The complementary to the unit 1.0 gives the same information in Pt. The important information lies in the proportion of spin current in Pt for small  $N$ . A typical value of about 10–50% of spin-current shunt in Pt for  $N < 17$  may lead to AHE sign inversion owing to a large value of SHA of Pt.

Figures 4(b) and 4(c) display both the local longitudinal conductivity  $\sigma_{xx}(z)$  (charge current density for

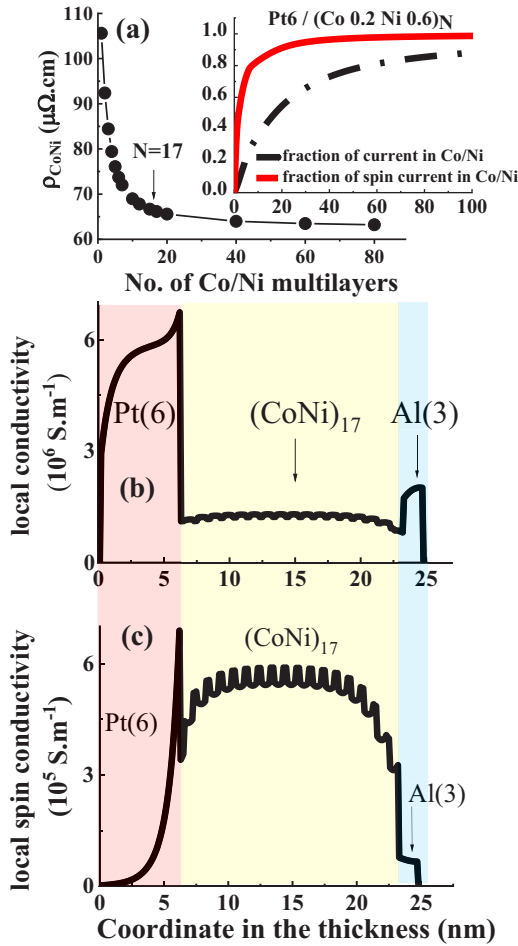


FIG. 4. (a) Average resistivity of  $(\text{Co}0.2/\text{Ni}0.6)_N$  vs number of Co/Ni repetitions induced by electronic interface scatterings. Inset: The fraction of current and spin current in Co/Ni multilayers in  $\text{Pt}(6)/(\text{Co}0.2/\text{Ni}0.6)_N$  systems showing a spin polarization of Pt as the total thickness of Co/Ni is small ( $N$  small). (b) Local conductivity in the  $\text{Pt}(6)/[\text{Co}/\text{Ni}]_{17}$  structure taking into account electronic interface scatterings. (c) Local spin conductivity in the  $\text{Pt}(6)/(\text{Co}/\text{Ni})_{17}$  structure, taking into account electronic interface scatterings. The physical parameters are given in Table I.

unit electric field) and local longitudinal spin conductivity  $\sigma_{xx}^z$  with magnetization along  $z$  for the corresponding  $\text{Pt}6/(\text{Co}0.2/\text{Ni}0.6)_N/\text{Al}3$  structure [Fig. 4(c)]. Those figures clearly display the shunt of the current in the Pt6 layer [Fig. 4(b)], owing to the higher conductivity of Pt compared to the thin-film Co/Ni layer together with the proximity leakage spin current in Pt and originating from Co/Ni; the transmission coefficient at the Co/Pt interface for the majority spin is set to unity with a full transmission specularity. The typical decrease of the spin current in Pt within 1 nm scales with the electronic mean free path. Such leakage spin current in Pt is responsible for the unconventional inverted anomalous Hall effect due to the opposite sign of the spin-orbit interaction between Pt and Co/Ni described here.

#### IV. DATA ANALYSIS AND INTERPRETATION

We now focus on the experimental results and quantitatively analyze the data using our theoretical basis. How do

we explain such observations? The spin current is generated in Co/Ni multilayers with a given spin polarization from the ferromagnetic bulk properties. However, as the number of sequences  $N$  for Co/Ni ( $N = 3-5$ ) remains small, the partly spin-polarized current becomes dominant in Pt compared to the Co/Ni region of reduced thickness. This occurs up to a given threshold limit of  $N$  above which the conduction becomes dominant in Co/Ni, like in the case of  $\text{Pt}/(\text{Co}/\text{Ni})_{20}$  and  $\text{Au}/\text{W}_{130}/(\text{Co}/\text{Ni})_{40}$  (Fig. 1). The semiphenomenological theory of current-in-plane (CIP) spin currents [86] indeed shows that Co/Ni is able to provide the necessary polarized current within all of the stacks, including Pt (Fig. 4). The existence of such spin-polarized proximity current is converted into a transverse current via the local SOI and ISHE. We thus demonstrate that Pt possesses a positive spin-Hall angle [19,29], while Co/Ni with thicker Ni possesses a negative SHE sign. This is corroborated by following the modeling and simulations presented in that second part.

#### A. Physical models for AHE

In order to retain the main physical principles driving the SHE and AHE in MLs with Pt-related interfaces, our idea is to distinguish the four possible different mechanisms of AHE in Co/Ni: (i) an *intrinsic* AHE-SHE phenomenon in Co/Ni viewed as an *effective* material and characterized by an average spin-Hall conductivity ( $\text{SHC} = \sigma_{xy}^{\text{int},s}$ ); and a pure *extrinsic* SHE mechanism acting either on (ii) the majority or (iii) the minority spin channels with an overall *extrinsic* SHA given by  $\theta^{\text{eff}} = \frac{\theta^{\uparrow}\sigma^{\uparrow} + \theta^{\downarrow}\sigma^{\downarrow}}{\sigma^{\uparrow} + \sigma^{\downarrow}}$ . A larger majority spin current is expected ( $\sigma^{\uparrow} > \sigma^{\downarrow}$ ), whereas a larger SHA is expected in the spin minority band ( $|\theta^{\uparrow}| < |\theta^{\downarrow}|$ ) by enhanced *sp-d* band mixing and the necessary phase shift for skew-scattering phenomena [93,98]. This brings uncertainties between scenarios (ii) and (iii) for the extrinsic mechanism as suggested in Refs. [39,94]. In that sense, our approach is slightly different from considering an identical SHA for both spin channels [56]. The last scenario (iv) is that of the magnetically induced moment in Pt (MPE) generating spin currents and AHE in Pt close to the Co interface at the scale of a few (typically 2) atomic planes [63–65].

Apart from spin-dependent electronic diffusions in bulk, one may emphasize the relevant boundary conditions to match for the out-of-equilibrium Fermi distribution in the framework of the Fuchs-Sondheimer model [84]. This is generally performed by including possible specular [88,89] or diffusive electron reflection (R) and transmission (T) at the interfaces in the CIP spin-dependent Boltzmann equations involving a layer- and spin-dependent electronic mean free path  $\lambda_i^s$ . One also has to consider the corresponding SOI spin-mixing terms in a  $2 \times 2$  Pauli matrix form and related spin-flip probability [99]. This is particularly true at the Co/Pt interface where the spin loss is known to be large. It is parameterized here by a spin-flip coefficient  $p_{sf}$  related to the spin-memory loss (SML)  $\delta$  parameter [19] according to  $p_{sf} = 1 - \exp(-\delta)$ . The SML at the 3d-5d interfaces plays an unavoidable role in spin pumping in ferromagnetic (FMR) experiments [19,69]. Moreover, one introduces the overall longitudinal resistivity

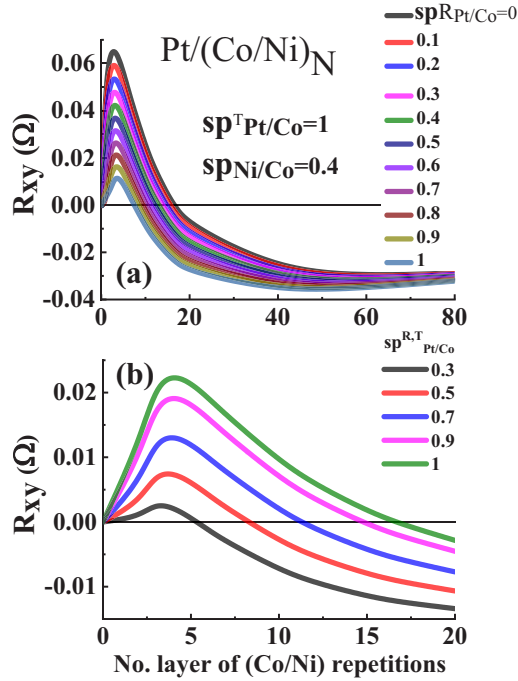


FIG. 5. (a) Anomalous Hall resistivity  $R_{xy}$  of Co/Ni in Pt(6)/(Co/Ni) $_N$  vs number of repetitions  $N$  calculated for different specularities of electron reflection at Co/Pt interfaces. The specularities of transmission at the Co/Pt interface is set to 1,  $sp_{Co/Pt}^T = 1$ , whereas at the Co/Ni interface, the values are fixed,  $sp_{Co/Ni}^T = sp_{Co/Ni}^R = 0.4$ . (b) Anomalous Hall resistivity of Pt(6)/(Co/Ni) $_N$  vs number of repetitions  $N$  of Co/Ni calculated for different specularities of reflection and transmission at the Co/Pt interfaces,  $sp_{Co/Pt}^T = sp_{Co/Pt}^R$ .

$\rho_{xx}^*$  (or conductivity  $\sigma_{xx}^*$ ) and transverse resistivities  $\rho_{xy}^*$  (or transverse conductivity  $\sigma_{xy}^*$ ) of the MLs as

$$R_{xx} = \rho_{xx}^* \frac{L}{Wt} \simeq \frac{L}{W} \frac{1}{t\sigma_{xx}^*} = \frac{L}{W} \frac{1}{\sum_{i,s} \sigma_{xx,i}^s t_i}, \quad (35)$$

$$R_{xy} \simeq \frac{\rho_{xy}^*}{t} = \frac{\sigma_{xy}^*}{t(\sigma_{xx}^*)^2} = \frac{\sum_{i,s} (\sigma_{xy,i}^s t_i)}{(\sum_{i,s} \sigma_{xx,i}^s t_i)^2}, \quad (36)$$

where  $L$ ,  $W$  represent the length and width of the Hall cross bars,  $t$  is the overall thickness of the MLs, and  $\sigma_{xx,i}^s$  is the local longitudinal spin conductivity of the  $i$ th layer of thickness  $t_i$  and  $\sigma_{xy,i}^s$  is the local off-diagonal spin conductivity of the  $i$ th layer.

### B. Effects of specularities on AHE

We now address, in detail, the effect of specularities on the unconventional AHE of Pt6/(Co/Ni) $_N$  structures with the help of our theory and calculations. Figure 5 displays our main results. We first show in Fig. 5(a) the effect of the specularities in reflection,  $sp_{Co/Pt}^R$ , of the Co/Pt interface, the transmission being fully specular as emphasized in Ref. [88]; the remaining parameters chosen for the simulations are given in Table I. One notes a clear decrease of the AHE resistivity  $R_{xy}$  as  $sp_{Co/Pt}^R$  increases from 0 to 1. This feature has to be associated to an increase of the spin current in Co/Ni only leading in parallel to a better compensation of the spin-charge

conversion between Co/Ni and Pt at small Co/Ni thickness, thus leading to a crossover from positive to negative AHE occurring for a smaller number of repetitions  $N$ .

In Fig. 5(b), we have changed both the specularities in reflection,  $sp_{Co/Pt}^R$ , and in transmission,  $sp_{Co/Pt}^T$ , at the Pt/Co interface in the same manner ( $sp_{Co/Pt}^R = sp_{Co/Pt}^T$ ) from 0.3 to 1. Compared to the previous case where  $sp_{Co/Pt}^T = 1$  and  $sp_{Co/Pt}^R = 0$ , one can observe that the  $R_{xy}$  signal drops from 0.06  $\Omega$  to 0.02  $\Omega$  for its maximal value, clearly indicating a reduction of the spin current injected into Pt from the Co/Ni ferromagnetic reservoir. The more  $sp_{Co/Pt}^T$  reduces to a small fraction, the less is the spin current in Pt, leading to a smaller positive AHE. The large specularities in transmission at the Co/Pt interface is then at the origin of the inverted AHE signal that one observes in both type-I and type-II sample series when  $N \simeq 3-10$  is small.

We now turn to the discussion of the specularities at Co/Ni interfaces (Fig. 6). We consider  $sp_{Co/Pt}^T = 1$  and  $sp_{Co/Pt}^R = 0$  for the Co/Pt interface corresponding to the optimum conditions for AHE sign inversion. Figure 6(a) displays the anomalous Hall resistance  $R_{xy}$  vs  $N = 1-100$  for different specularities at reflection for each Co/Ni interface ( $sp_{Co/Ni}^R$ ) with full transmission. Figure 6(b) represents the dependence of  $R_{xy}$  on the specularities on transmission at Co/Ni ( $sp_{Co/Ni}^T$ ) without reflection, whereas Fig. 6(c) is the result of joint variation of  $sp_{Co/Ni}^R$  and  $sp_{Co/Ni}^T = sp_{Co/Ni}^R = sp_{Co/Ni}$ .

Three main remarks can be appended. (i) For small  $N$ , one still observes, in any case, a sign inversion of AHE, which is positive in the case of Pt dominant spin-charge conversion and opposite compared to Co/Ni. (ii) The AHE resistance in the region of spin-charge conversion inversion (small  $N$ ) increases when the electron specularities at reflection [Fig. 6(a)] and at transmission [Fig. 6(b)] at Co/Ni interfaces  $sp_{Co/Ni}^{R,T}$  increases from 0 to 1. This indicates a larger spin current in Co/Ni, thereby injected into Pt by the transport proximity effect. (iii) On the other hand, the increase of the spin current in Co/Ni volume upon the increase of  $sp_{Co/Ni}^{R,T}$  makes the crossover from positive to negative AHE appear at a smaller value of  $N$ . This should be linked to a larger mean free path of Co/Ni (Co and Ni) compared to Pt. In the end, a joint increase of the specularities in transmission and in reflection [Fig. 6(c)] gives rise to the same trends as developed in case (ii) and then to the same conclusions.

*Magnetic proximity effects.* Moreover, from those simulations, we have performed a different treatment for the integral of the spin-charge conversion in Pt and the results are displayed at the bottom of Fig. 7. We have, respectively, applied a certain cutoff in the integral up to, respectively,  $z_{\text{cutoff}} = 0.4, 0.6, 1.6, 6.0$  nm. This cutoff should mimic the possible role of the magnetic proximity effect in Pt leading to an induced magnetic moment in Pt over typically two or three atomic planes. One observes that using the tabulated parameters in Table I, the experimental data may be recovered only when the integral is made on a total thickness of 1.6 or 6.0 nm, which is much larger than the 0.6 nm corresponding to the thickness of three atomic planes of Pt. With varying the physical parameters, we were not able to fit the experimental data by using a cutoff of 0.6 nm together with a crossover occurring at  $N = 17$ , unless considering a spin-Hall angle of



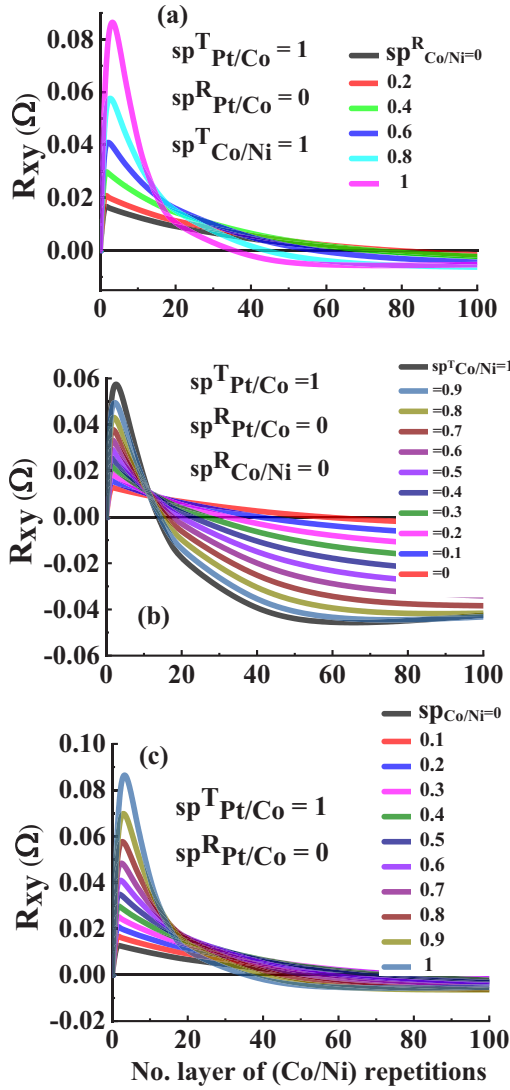


FIG. 6. (a) Anomalous Hall resistivity  $R_{xy}$  vs number of repetitions  $N$  of Co/Ni in Pt(6)/(Co/Ni) $_N$  calculated for different specularities of electron reflection at Co/Ni interfaces. The specularities for transmission at Co/Pt (reflection) and Co/Ni interfaces is set to 1 (0). (b) Anomalous Hall resistivity vs number of repetitions  $N$  of Co/Ni in Pt(6)/(Co/Ni) $_N$  calculated for different specularities of transmission at the Co/Ni interfaces. The specularities at reflection at the Co/Ni interfaces is set to 0, whereas the specularities at transmission for the Co/Pt interface is set to 1. (c) Anomalous Hall resistivity vs number of repetitions  $N$  of Co/Ni in Pt(6)/(Co/Ni) $_N$  for different joint variations of specularities at reflection and transmission for Co/Ni  $sp^R_{Co/Pt} = sp^T_{Co/Pt}$ .

Pt larger than 60%. This shows that the spin-current proximity effect is the main cause for the inverted anomalous Hall effect that we observe here.

## V. RESULTS OF DATA FITTING AND CONCLUSIONS

Two different cases may now be distinguished according to the (i) *extrinsic* or the (ii) and (iii) *intrinsic* nature of the AHE here. For cases (ii) and (iii),  $\sigma_{xy,i}$  may be expressed as  $\sum_s \theta_i^s \sigma_{xx,i}^s$  for both ferromagnetic and normal metals, with  $\theta_i^s$

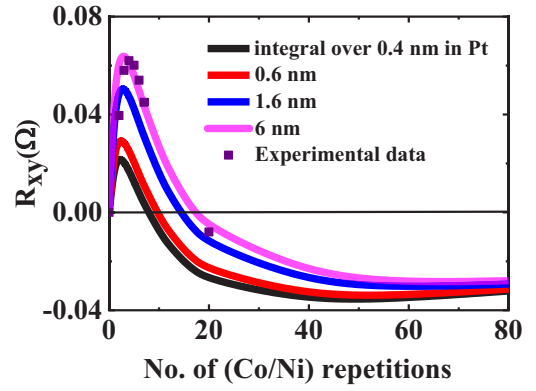


FIG. 7. Anomalous Hall resistivity vs number of repetitions  $N$  of Co/Ni in Pt(6)/(Co/Ni) $_N$  vs the cutoff of the integral of the spin-to-charge conversion in the Pt thickness from the Pt/Co interface. Squares represent the experimental data for the type-II Pt series.

the local spin-Hall angle of layer  $i$  for the  $s$ -spin channel [39]. One has  $\theta_i^\downarrow = -\theta_i^\uparrow$  for nonmagnetic materials, whereas no equivalent relationship exists for a ferromagnet because of the spin-degeneracy lift making  $\theta^\uparrow$  and  $\theta^\downarrow$  different in absolute value [39]. However, one may generally assume that  $\theta_i^\downarrow$  and  $\theta_i^\uparrow$  are of opposite sign. For those calculations, the current density for the  $s$ -spin channel in the MLs is calculated via the relationship given by Eq. (22) where  $g^s(z, v_z)$  are the out-of-equilibrium Fermi distributions for spin  $s$ , which is the solution of the Boltzmann equation within the MLs,  $v_{x,z}$  is the Fermi velocity along the current direction ( $x$ ) or along the perpendicular ( $z$ ) to the layers, and  $S$  is the section.  $g^s(z, v_z)$  possess two components, i.e., one for the bulk and the other decreasing in  $z$  related to the spin-dependent scattering at the interfaces that should be found self-consistently. After integration of Eq. (22), one has access to  $\sigma_{xx,i}^s$  and  $\sigma_{xy,i}^s$ , respectively. The transverse current is calculated by considering the local transverse conductivity and by summing all contributions.

On the basis of the aforementioned arguments of the *extrinsic vs intrinsic* SHE mechanism in Co/Ni, we have proceeded to the four different fitting procedures for AHE in the Pt and Au:W series and retained the best fit. We refer to Fig. 3(b) for the resulting fits with the different set of parameters given in Table I. In the present case, SML is taken into account in the interfacial scattering matrix at each Pt/Co (with  $\delta = 0.9$  [19,69,100] or, equivalently,  $p_{sf} = 0.6$ ) and Co/Ni (with  $\delta = 0.25$  or, equivalently,  $p_{sf} = 0.3$ ) interfaces as given in Ref. [97]. The fits have been obtained with a SHA for Pt equal to  $\theta_{Pt} = \theta_{Pt}^\uparrow = -\theta_{Pt}^\downarrow = +20 \pm 2\%$ ,  $\theta_{Au:W_{80}} = +10 \pm 1\%$ , and  $\theta_{Au:W_{130}} = -0.3 \pm 0.1\%$ , whereas the different models yield the following (see Table I):

(i) *intrinsic* SHE mechanism in Co/Ni, giving  $\sigma_{xy}^{int} = -85 \text{ S cm}^{-1}$ ;

(ii) *extrinsic* SHE mechanism in Co/Ni on the majority spin-channel effect, giving  $\theta_{(Co/Ni)}^\uparrow = -0.9\%$  ( $\theta_{(Co/Ni)}^\downarrow = 0$ ) [blue fit in Fig. 3(b)];

(iii) *extrinsic* SHE mechanism in Co/Ni on the minority spin-channel effect, giving  $\theta_{(Co/Ni)}^\downarrow = -2.2\%$  ( $\theta_{(Co/Ni)}^\uparrow = 0$ ) [purple-dot fit in Fig. 3(b)].

(iv) The conductivity for Co/Ni,  $\sigma_{xy}^{int}$ , should be compared to the extrinsic one with balanced spin-Hall effect

on both the spin-up and spin-down channel,  $\theta_{(Co/Ni)}^\uparrow = -\theta_{(Co/Ni)}^\downarrow = -1.5\%$ , with the corresponding relationship  $\sigma_{xy}^{\text{int.}} \simeq \theta_{(Co/Ni)} \mathcal{P} \sigma_{xx}$  with  $\mathcal{P} \sigma_{xx} = \sigma_{xx}^\uparrow - \sigma_{xx}^\downarrow$  [green fit in Fig. 3(b)].

The equivalent spin conductivity extracted from the *extrinsic* model may be estimated at the vicinity of  $-75 \text{ S cm}^{-1}$  for  $N = 17$ , which is close and then in numerical agreement with case (i) of *intrinsic* conductivity. The  $N = 17$  sample corresponds to an equal transverse charge current in Pt and Co/Ni, giving the condition  $\theta_{\text{Pt}} \times \Phi_{\text{Pt}}^s = \theta_{(Co/Ni)} \times \Phi_{(Co/Ni)}^s$  for  $N = 17$ , where  $\Phi^s$  represents the respective fraction of the spin current in Pt and in Co/Ni with  $\Phi_{\text{Pt}}^s + \Phi_{(Co/Ni)}^s = 1$ . A value of  $\Phi_{\text{Pt}}^s = 0.07$  as calculated for  $N = 17$  gives a ratio of about 13 between the spin-Hall angles of Pt and Co/Ni, like extracted from our fit procedure. Figure 3(a) displays the fits between the experiment value of  $R_{xy}$  and the model for Au:W<sub>130</sub>/(Co/Ni) and Au:W<sub>80</sub>/(Co/Ni) obtained with  $\theta_{\text{Au:W}_{130}} = -0.3\%$  and  $\theta_{\text{Au:W}_{80}} = +10\%$  as experimentally determined in a previous work [29]. Note that for both series of samples, at very high number of repetitions  $N$  ( $N = 250$ ),  $R_{xy}$  of Pt/(Co/Ni) and Au:W/(Co/Ni) merge together towards the intrinsic value of AHE in (Co/Ni), equaling  $R_{xy} = -17 \text{ m}\Omega$ . The respective transverse  $\rho_{xy}^*$  in Eq. (36) and longitudinal resistivity  $\rho_{xx}^*$  in Eq. (2) are also compared to the experimental data in Fig. 2, showing a very good agreement.

Although one cannot discriminate between the extrinsic and intrinsic models and simulations for AHE concerning Co/Ni for that range of  $N = 3-40$  and bilayer thicknesses, two major conclusions may be raised. The first one is that in any case, the consistent spin-Hall angle of Pt,  $+20\%$ , is observed to be clearly enhanced compared to its value extracted from spin pumping–ISHE experiments [19]. No admissible fits may be obtained with typical SHA values for Pt inferior to  $20\%$ . Such enhancement of the spin-Hall angle in Pt has already been observed in Spin-transfer torque (STT-FMR) experiments [20,67–69], lateral spin-valve (LSV) geometry, as well as spin-Hall magnetoresistance with Co/Pt [101]. This particularly large value of  $\theta_{\text{Pt}}$  may account for an anisotropy of the electronic scattering time close to the interface. Beyond the change of the intrinsic SHE properties by disorder or energy broadening [70], electron anisotropic scattering may

have the effect of enhancing the intrinsic SHA. The second important issue is the magnetic proximity effect: one clearly cannot converge towards a reasonable fit to data when one considers the spin-current integration in space limited to two to three Pt atomic planes at the interface with Co, unless one considers a value of SHA in Pt of the order of  $60-80\%$ . We consider that the magnetic proximity effect of such origin for the AHE inversion that we observe cannot play the main role.

In conclusion, we evidenced an inverted anomalous Hall effect in Co/Ni-based multilayers grown on a thin Pt buffer via spin-polarized transport proximity, i.e., spin-current leakage effects. The model and simulations are strongly dependent on the basics electronic transport properties. Using advanced simulation methods for the description of the current and spin-current profiles within multilayers, we have shown that the electronic specularly in reflection and in transmission at inner interfaces and outward surfaces responsible for the increase of resistivity makes the AHE of thin films and thin multilayers very dependent on the layers' quality. We have highlighted opposite spin-Hall angles for Pt and Co/Ni and the relevant transport parameters. The sizable SHA extracted for Pt,  $+20\%$ , is opposite to the one of Co/Ni, giving rise to AHE inversion for thin Co/Ni multilayers. The large SHA of Pt cannot be explained by spin-current proximity effects, and is found to be larger than previously measured in spin pumping–ISHE experiments, an effect that may originate from the anisotropy of the electron scattering time in the multilayers. Moreover, we can conclude that the AHE data combined with advanced simulation methods may probe the main properties of the interfacial spin-orbit interactions in metals.

## ACKNOWLEDGMENTS

This work was supported by the French Agence Nationale de la Recherche through the ANR Project TOPRISE No. ANR-16-CE24-0017. We acknowledge financial support from the Horizon 2020 Framework Programme of the European Commission under FET-Open Grant Agreement No. 863155 (s-Nebula). T.H.D. acknowledges the Horizon 2020 Framework Programme of the European Commission under FET-Proactive Grant Agreement No. 824123 (SKYTOP).

- 
- [1] L. Liu, T. Moriyama, D. C. Ralph, and R. A. Buhrman, Spin-Torque Ferromagnetic Resonance Induced by the Spin Hall Effect, *Phys. Rev. Lett.* **106**, 036601 (2011).
  - [2] L. Liu, C.-F. Pai, D. C. Ralph, and R. A. Buhrman, Magnetic Oscillations Driven by the Spin-Hall Effect in 3-Terminal Magnetic Tunnel Junction Devices, *Phys. Rev. Lett.* **109**, 186602 (2012).
  - [3] L. Liu, C.-F. Pai, Y. Li, H. W. Tseng, D. C. Ralph, and R. A. Buhrman, Spin-torque switching with the giant spin hall effect of tantalum, *Science* **336**, 555 (2012).
  - [4] C. F. Pai, L. Liu, Y. Li, H. W. Tseng, D. C. Ralph, and R. A. Buhrman, Spin transfer torque devices utilizing the giant spin Hall effect of tungsten, *Appl. Phys. Lett.* **101**, 122404 (2012).
  - [5] B. Jinnai, C. Zhang, A. Kurenkov, M. Bersweiler, H. Sato, S. Fukami, and H. Ohno, Spin-orbit torque induced magnetization switching in Co/Pt multilayers, *Appl. Phys. Lett.* **111**, 102402 (2017).
  - [6] I. M. Miron, K. Garello, G. Gaudin, P.-J. Zermatten, M. V. Costache, S. Auffret, S. Bandiera, B. Rodmacq, A. Schuhl, and P. Gambardella, Perpendicular switching of a single ferromagnetic layer induced by in-plane current injection, *Nature* **476**, 189 (2011).
  - [7] O. Boulle, S. Rohart, L. D. Buda-Prejbeanu, E. Jué, I. M. Miron, S. Pizzini, J. Vogel, G. Gaudin, and A. Thiaville, Domain Wall Tilting in the Presence of the Dzyaloshinskii-Moriya Interaction in Out-of-Plane Magnetized Magnetic Nanotracks, *Phys. Rev. Lett.* **111**, 217203 (2013).

- [8] S. Emori, U. Bauer, S. M. Ahn, E. Martinez, and G. S. D. Beach, Current-driven dynamics of chiral ferromagnetic domain walls, *Nat. Mater.* **12**, 611 (2013).
- [9] S. Parkin, S. Yang, and K. Ryu, Domain-wall velocities of up to 750 m/s driven by exchange-coupling torque in synthetic antiferromagnets, *Nat. Nano.* **10**, 221 (2015).
- [10] J.-C. Rojas-Sánchez, P. Laczkowski, J. Sampaio, S. Collin, K. Bouzehouane, N. Reyren, H. Jaffrès, A. Mougin, and J.-M. George, Perpendicular magnetization reversal in Pt/[Co/Ni]<sub>3</sub>/Al multilayers via the spin Hall effect of Pt, *Appl. Phys. Lett.* **108**, 082406 (2016).
- [11] M. Baumgartner, K. Garello, J. Mendil, C. O. Avci *et al.*, Spatially and time-resolved magnetization dynamics driven by spin-orbit torques, *Nat. Nano.* **12**, 980 (2017).
- [12] S. Fukami, T. Suzuki, H. Tanigawa, N. Ohshima, and N. Ishiwata, Stack structure dependence of co/ni multilayer for current-induced domain wall motion, *Appl. Phys. Expt.* **3**, 113002 (2010).
- [13] J.-Y. Chauléau, W. Legrand, N. Reyren, D. Maccariello, S. Collin, H. Popescu, K. Bouzehouane, V. Cros, N. Jaouen, and A. Fert, Chirality in Magnetic Multilayers Probed by the Symmetry and the Amplitude of Dichroism in x-ray Resonant Magnetic Scattering, *Phys. Rev. Lett.* **120**, 037202 (2018).
- [14] J. Walowski and M. Münzenberg, Perspective: Ultrafast magnetism and THz spintronics, *J. Appl. Phys.* **120**, 140901 (2016).
- [15] N. Nagaosa, J. Sinova, S. Onoda, A. H. MacDonald, and N. P. Ong, Anomalous Hall effects, *Rev. Mod. Phys.* **82**, 1539 (2010).
- [16] J. Sinova, S. O. Valenzuela, J. Wunderlich, C. H. Back, and T. Jungwirth, Spin Hall effects, *Rev. Mod. Phys.* **87**, 1213 (2015).
- [17] F. Hellman, A. Hoffmann, Y. Tserkovnyak, G. S. D. Beach, E. E. Fullerton, C. Leighton, A. H. MacDonald, D. C. Ralph, D. A. Arena, H. A. Durr, P. Fischer, J. Grollier, J. P. Heremans, T. Jungwirth, A. V. Kimel, B. Koopmans, I. N. Krivorotov, S. J. May, A. K. Petford-Long, J. M. Rondinelli, N. Samarth, I. K. Schuller, A. N. Slavin, M. D. Stiles, O. Tchernyshyov, A. Thiaville, and B. L. Zink, Interface-induced phenomena in magnetism, *Rev. Mod. Phys.* **89**, 025006 (2017).
- [18] A. Hoffmann, Spin Hall effects in metals, *IEEE Trans. Magn.* **49**, 5172 (2013).
- [19] J.-C. Rojas-Sánchez, N. Reyren, P. Laczkowski, W. Savero, J.-P. Attané, C. Deranlot, M. Jamet, J. M. George, L. Vila, and H. Jaffrès, Spin Pumping and Inverse Spin Hall Effect in Platinum: The Essential role of Spin-Memory Loss at Metallic Interfaces, *Phys. Rev. Lett.* **112**, 106602 (2014).
- [20] W. Zhang, W. Han, X. Jiang, S. H. Yang, and S. S. P. Parkin, Role of transparency of platinum-ferromagnet interfaces in determining the intrinsic magnitude of the spin Hall effect, *Nat. Phys.* **11**, 496 (2015).
- [21] C. F. Pai, Y. Ou, L. H. Vilela-Leão, D. C. Ralph, and R. A. Buhrman, Dependence of the efficiency of spin hall torque on the transparency of Pt/ferromagnetic layer interfaces, *Phys. Rev. B* **92**, 064426 (2015).
- [22] E. Sagasta, Y. Omori, M. Isasa, M. Gradhand, L. E. Hueso, Y. Niimi, Y. Otani, and F. Casanova, Tuning the spin Hall effect of Pt from the moderately dirty to the superclean regime, *Phys. Rev. B* **94**, 060412 (2016).
- [23] Q. Hao and G. Xiao, Giant Spin Hall Effect and Switching Induced by Spin-Transfer Torque in a W/Co<sub>40</sub>Fe<sub>40</sub>B<sub>20</sub>/MgO Structure with Perpendicular Magnetic Anisotropy, *Phys. Rev. Appl.* **3**, 034009 (2015).
- [24] Y. Niimi, M. Morota, D. H. Wei, C. Deranlot, M. Basletic, A. Hamzic, A. Fert, and Y. Otani, Extrinsic Spin Hall Effect Induced by Iridium Impurities in Copper, *Phys. Rev. Lett.* **106**, 126601 (2011).
- [25] Y. Niimi, Y. Kawanishi, D. H. Wei, C. Deranlot, H. X. Yang, M. Chshiev, T. Valet, A. Fert, and Y. Otani, Giant Spin Hall Effect Induced by Skew Scattering from Bismuth Impurities Inside Thin Film Cubic Alloys, *Phys. Rev. Lett.* **109**, 156602 (2012).
- [26] P. Laczkowski, J.-C. Rojas-Sánchez, W. Savero-Torres, H. Jaffrès, N. Reyren, C. Deranlot, L. Notin, C. Beigné, A. Marty, J.-P. Attané, L. Vila, J. M. George, and Albert Fert, Experimental evidences of a large extrinsic spin Hall effect in AuW alloy, *Appl. Phys. Lett.* **104**, 142403 (2014).
- [27] P. Laczkowski, H. Jaffrès, W. Savero-Torres, J. C. Rojas-Sanchez, Y. Fu, N. Reyren, C. Deranlot, L. Notin, C. Beigne, J. P. Attane, L. Vila, J. M. George, and A. Marty, Evaluation of spin diffusion length of AuW alloys using spin absorption experiments in the limit of large spin-orbit interactions, *Phys. Rev. B* **92**, 214405 (2015).
- [28] M. Obstbaum, M. Decker, A. K. Greitner, M. Haertinger, T. N. G. Meier, M. Kronseder, K. Chadova, S. Wimmer, D. Kodderitzsch, H. Ebert, and C. H. Back, Tuning Spin Hall Angles by Alloying, *Phys. Rev. Lett.* **117**, 167204 (2016).
- [29] P. Laczkowski, Y. Fu, H. Yang, J. C. Rojas-Sanchez, P. Noel, V. T. Pham, G. Zahnd, C. Deranlot, S. Collin, C. Bouard, P. Warin, V. Maurel, M. Chshiev, A. Marty, J. P. Attane, A. Fert, H. Jaffrès, L. Vila, and J. M. George, Large enhancement of the spin Hall effect in Au by side-jump scattering on Ta impurities, *Phys. Rev. B* **96**, 140405(R) (2017).
- [30] L. Zhu, D. C. Ralph, and R. A. Buhrman, Highly Efficient Spin-Current Generation by the Spin Hall Effect in Au<sub>1-x</sub>Pt<sub>x</sub>, *Phys. Rev. Appl.* **10**, 031001 (2018).
- [31] L. Zhu, L. Zhu, S. Shi, M. Sui, D. C. Ralph, and R. Buhrman, Enhancing Spin-Orbit Torque by Strong Interfacial Scattering from Ultrathin Insertion Layers, *Phys. Rev. Appl.* **11**, 061004 (2019).
- [32] L. Zhu, L. Zhu, M. Sui, D. C. Ralph, and R. A. Buhrman, Variation of the giant intrinsic spin hall conductivity of Pt with carrier lifetime, *Sci. Adv.* **5**, eaav8025 (2019).
- [33] P. M. Levy, H. Yang, M. Chshiev, and A. Fert, Spin Hall effect induced by bi impurities in Cu: Skew scattering and side-jump, *Phys. Rev. B* **88**, 214432 (2013).
- [34] R. Karplus and J. M. Luttinger, Hall effect in ferromagnetics, *Phys. Rev.* **95**, 1154 (1954).
- [35] J. Smit, The spontaneous Hall effect in ferromagnetics I, *Physica* **21**, 877 (1955).
- [36] J. Smit, The spontaneous Hall effect in ferromagnetics II, *Physica* **24**, 39 (1958).
- [37] L. Berger, Side-jump mechanism for the hall effect of ferromagnets, *Phys. Rev. B* **2**, 4559 (1970).
- [38] A. Fert and O. Jaoul, Left-Right Asymmetry in the Scattering of Electrons by Magnetic Impurities, and a Hall Effect, *Phys. Rev. Lett.* **28**, 303 (1972).
- [39] A. Fert, A. Friederich, and A. Hamzic, Hall effect in dilute magnetic alloys, *J. Magn. Mater.* **24**, 231 (1981).

- [40] W. Vavra, C. H. Lee, F. J. Lamelas, H. He, R. Clarke, and C. Uher, Magnetoresistance and Hall effect in epitaxial Co-Au superlattices, *Phys. Rev. B* **42**, 4889 (1990).
- [41] S. Kim, S. R. Lee, and J. D. Chung, Magnetic properties of Pd/Co multilayer films studied by Hall effect, *J. Appl. Phys.* **73**, 6344 (1993).
- [42] O. Shaya, M. Karpovskii, and A. Gerber, Extraordinary Hall effect in Co-Pd bilayers, *J. Appl. Phys.* **102**, 043910 (2007).
- [43] D. Rosenblatt, M. Karpovskii, and A. Gerber, Reversal of the extraordinary Hall effect polarity in thin Co/Pd multilayers, *Appl. Phys. Lett.* **96**, 022512 (2010).
- [44] Z. B. Guo, W. B. Mi, R. O. Aboljadayel, B. Zhang, Q. Zhang, P. G. Barba, A. Manchon, and X. X. Zhang, Effects of surface and interface scattering on anomalous Hall effect in Co/Pd multilayers, *Phys. Rev. B* **86**, 104433 (2012).
- [45] X. Kou, J.-M. Schmalhorst, V. Keskin, and G. Reiss, Magnetic anisotropy and anomalous Hall effect of ultrathin Co/Pd bilayers, *J. Appl. Phys.* **112**, 093915 (2012).
- [46] V. Keskin, B. Aktas, J. Schmalhorst, G. Reiss, H. Zhang, J. Weischenberg, and Y. Mokrousov, Temperature and Co thickness dependent sign change of the anomalous Hall effect in Co/Pd multilayers: An experimental and theoretical study, *Appl. Phys. Lett.* **102**, 022416 (2013).
- [47] C. L. Canedy, X. W. Li, and G. Xiao, Extraordinary Hall effect in (111) and (100)-orientated Co/Pt superlattices, *J. Appl. Phys.* **81**, 5367 (1997).
- [48] C. L. Canedy, X. W. Li, and G. Xiao, Large magnetic moment enhancement and extraordinary Hall effect in Co/Pt superlattices, *Phys. Rev. B* **62**, 508 (2000).
- [49] P. Zhang, K. Xie, W. Lin, D. Wu, and H. Sang, Anomalous Hall effect in Co/Ni multilayers with perpendicular magnetic anisotropy, *Appl. Phys. Lett.* **104**, 082404 (2014).
- [50] M. Arora, R. Hübner, D. Suess, B. Heinrich, and E. Girt, Origin of perpendicular magnetic anisotropy in Co/Ni multilayers, *Phys. Rev. B* **96**, 024401 (2017).
- [51] L. Zhu, D. C. Ralph, and R. A. Buhrman, Spin-Orbit Torques in Heavy-Metal-Ferromagnet Bilayers with Varying Strengths of Interfacial Spin-Orbit Coupling, *Phys. Rev. Lett.* **122**, 077201 (2019).
- [52] T. Tanaka, H. Kontani, M. Naito, T. Naito, D. S. Hirashima, K. Yamada, and J. Inoue, Intrinsic spin Hall effect and orbital Hall effect in  $4d$  and  $5d$  transition metals, *Phys. Rev. B* **77**, 165117 (2008).
- [53] G. Y. Guo, S. Murakami, T.-W. Chen, and N. Nagaosa, Intrinsic Spin Hall Effect in Platinum: First-Principles Calculations, *Phys. Rev. Lett.* **100**, 096401 (2008).
- [54] A. Hönemann, C. Herschbach, D. V. Fedorov, M. Gradhand, and I. Mertig, Spin and charge currents induced by the spin Hall and anomalous Hall effects upon crossing ferromagnetic/nonmagnetic interfaces, *Phys. Rev. B* **99**, 024420 (2019).
- [55] A. Hönemann, C. Herschbach, D. V. Fedorov, M. Gradhand, and I. Mertig, Absence of strong skew scattering in crystals with multi-sheeted Fermi surfaces, *J. Phys. Cond. Mater.* **31**, 085803 (2019).
- [56] Y. Omori, E. Sagasta, Y. Niimi, M. Gradhand, L. E. Hueso, F. Casanova, and Y. Otani, Relation between spin Hall effect and anomalous Hall effect in  $3d$  ferromagnetic metals, *Phys. Rev. B* **99**, 014403 (2019).
- [57] Y. Hibino, K. Yakushiji, A. Fukushima, H. Kubota, and S. Yuasa, Spin-orbit torque generated from perpendicularly magnetized Co/Ni multilayers, *Phys. Rev. B* **101**, 174441 (2020).
- [58] T. Y. Ma, C. H. Wan, X. Wang, W. L. Yang, C. Y. Guo, C. Fang, M. K. Zhao, J. Dong, Y. Zhang, and X. F. Han, Evidence of magnetization switching by anomalous spin Hall torque in NiFe, *Phys. Rev. B* **101**, 134417 (2020).
- [59] V. P. Amin, J. Zemen, and M. D. Stiles, Interface-Generated Spin Currents, *Phys. Rev. Lett.* **121**, 136805 (2018).
- [60] A. Davidson, V. P. Amin, W. S. Aljuaid, P. M. Haney, and X. Fan, Perspectives of electrically generated spin currents in ferromagnetic materials, *Phys. Lett. A* **384**, 126228 (2020).
- [61] H. Hayashi, A. Asami, and K. Ando, Anomalous Hall effect at a Pt/Co interface, *Phys. Rev. B* **100**, 214415 (2019).
- [62] Q. Zhang, D. Zheng, Y. Wen, Y. Zhao, W. Mi, A. Manchon, O. Boulle, and X. Zhang, Effect of surface roughness on the anomalous Hall effect in Fe thin films, *Phys. Rev. B* **101**, 134412 (2020).
- [63] W. Zhang, M. B. Jungfleisch, W. Jiang, Y. Liu, J. E. Pearson, S. G. E. T. Velthuis, A. Hoffmann, F. Freimuth, and Y. Mokrousov, Reduced spin-Hall effects from magnetic proximity, *Phys. Rev. B* **91**, 115316 (2015).
- [64] M. Caminale, A. Ghosh, S. Auffret, U. Ebels, K. Ollefs, F. Wilhelm, A. Rogalev, and W. E. Bailey, Spin pumping damping and magnetic proximity effect in Pd and Pt spin-sink layers, *Phys. Rev. B* **94**, 014414 (2016).
- [65] T. A. Peterson, A. P. McFadden, C. J. Palmström, and P. A. Crowell, Influence of the magnetic proximity effect on spin-orbit torque efficiencies in ferromagnet/platinum bilayers, *Phys. Rev. B* **97**, 020403 (2018).
- [66] K. Gupta, R. J. H. Wesselink, R. Liu, Z. Yuan, and P. J. Kelly, Disorder Dependence of Interface Spin Memory Loss, *Phys. Rev. Lett.* **124**, 087702 (2020).
- [67] H. Nguyen, W. Pratt, and J. Bass, Spin-flipping in Pt and Co/Pt interfaces, *J. Magn. Magn. Mater.* **361**, 30 (2014).
- [68] C. T. Boone, J. M. Shaw, H. T. Nembach, and T. J. Silva, Spin-scattering rates in metallic thinfilms measured by ferromagnetic resonance damping enhanced by spin-pumping, *J. Appl. Phys.* **117**, 223910 (2015).
- [69] A. J. Berger, E. R. J. Edwards, H. T. Nembach, O. Karis, M. Weiler, and T. J. Silva, Determination of the spin Hall effect and the spin diffusion length of Pt from self-consistent fitting of damping enhancement and inverse spin-orbit torque measurements, *Phys. Rev. B* **98**, 024402 (2018).
- [70] H. Kontani, T. Tanaka, and K. Yamada, Intrinsic anomalous Hall effect in ferromagnetic metals studied by the multi- $d$ -orbital tight-binding model, *Phys. Rev. B* **75**, 184416 (2007).
- [71] M.-H. Nguyen, D. C. Ralph, and R. A. Buhrman, Spin Torque Study of the Spin Hall Conductivity and Spin Diffusion Length in Platinum Thin Films with Varying Resistivity, *Phys. Rev. Lett.* **116**, 126601 (2016).
- [72] D. Ködderitzsch, K. Chadova, and H. Ebert, Linear response Kubo-Bastin formalism with application to the anomalous and spin Hall effects: A first-principles approach, *Phys. Rev. B* **92**, 184415 (2015).
- [73] K. Chadova, D. V. Fedorov, C. Herschbach, M. Gradhand, I. Mertig, D. Ködderitzsch, and H. Ebert, Separation of the individual contributions to the spin Hall effect in dilute alloys



- within the first-principles Kubo-Streda approach, *Phys. Rev. B* **92**, 045120 (2015).
- [74] J. Kötzer and W. Gil, Anomalous Hall resistivity of cobalt films: Evidence for the intrinsic spin-orbit effect, *Phys. Rev. B* **72**, 060412 (2005).
- [75] D. Hou, Y. Li, D. Wei, D. Tian, L. Wu, and X. Jin, The anomalous Hall effect in epitaxial face-centered-cubic cobalt films, *J. Phys.: Cond. Mater.* **24**, 482001 (2012).
- [76] J. M. Lavine, Extraordinary Hall-effect measurements on Ni, some Ni alloys, and ferrites, *Phys. Rev.* **123**, 1273 (1961).
- [77] L. Ye, Y. Tian, X. Jin, and D. Xiao, Temperature dependence of the intrinsic anomalous Hall effect in nickel, *Phys. Rev. B* **85**, 220403 (2012).
- [78] X. Wang, D. Vanderbilt, J. R. Yates, and I. Souza, Fermi-surface calculation of the anomalous Hall conductivity, *Phys. Rev. B* **76**, 195109 (2007).
- [79] E. Roman, Y. Mokrousov, and I. Souza, Orientation Dependence of the Intrinsic Anomalous Hall Effect in hcp Cobalt, *Phys. Rev. Lett.* **103**, 097203 (2009).
- [80] I. Turek, J. Kudrnovský, and V. Drchal, *Ab initio* theory of galvanomagnetic phenomena in ferromagnetic metals and disordered alloys, *Phys. Rev. B* **86**, 014405 (2012).
- [81] J. Weischenberg, F. Freimuth, J. Sinova, S. Blügel, and Y. Mokrousov, *Ab initio* theory of the Scattering-Independent Anomalous Hall Effect, *Phys. Rev. Lett.* **107**, 106601 (2011).
- [82] S. Mizukami, X. Zhang, T. Kubota, H. Naganuma, M. Oogane, Y. Ando, and T. Miyazaki, Gilbert damping in Ni/Co multilayer films exhibiting large perpendicular anisotropy, *Appl. Phys. Expt.* **4**, 013005 (2011).
- [83] K.-S. Ryu, S.-H. Yang, L. Thomas, and S. S. P. Parkin, Chiral spin torque arising from proximity-induced magnetization, *Nat. Commun.* **5**, 3910 (2014).
- [84] E. Sondheimer, The mean free path of electrons in metals, *Adv. Phys.* **1**, 1 (1952).
- [85] O. C. V. Stejskal, A. Thiaville, J. Hamrle, S. Fukami, and H. Ohno, Current distribution in metallic multilayers from resistance measurements, *Phys. Rev. B* **101**, 235437 (2020).
- [86] R. E. Camley and J. Barnas, Theory of Giant Magnetoresistance Effects in Magnetic Layered Structures with Antiferromagnetic Coupling, *Phys. Rev. Lett.* **63**, 664 (1989).
- [87] X.-G. Zhang and W. H. Butler, Conductivity of metallic films and multilayers, *Phys. Rev. B* **51**, 10085 (1995).
- [88] D. A. Stewart, W. H. Butler, X.-G. Zhang, and V. F. Los, Interfacial scattering in magnetic multilayers and spin valves, *Phys. Rev. B* **68**, 014433 (2003).
- [89] K. Chen and S. Zhang, Roles of nonlocal conductivity on spin Hall angle measurement, *Phys. Rev. B* **96**, 134401 (2017).
- [90] See Supplemental Material at <http://link.aps.org/supplemental/10.1103/PhysRevB.102.144405> for discussions about the sign and magnitude of the ordinary Hall effect (OHE) acquired at low temperature on the different samples (part I), and on the discussion of spin-orbit assisted electron scattering and CIP-spin currents (part II).
- [91] N. V. Volkenshtein and G. V. Fedorov, Temperature dependence of the Hall effect of pure ferromagnets, *J. Exptl. Theoret. Phys. (U.S.S.R.)* **38**, 64 (1960) [*Soviet Phys. JETP* **11**, 48 (1960)].
- [92] H. Wu, S. A. Razavi, Q. Shao, X. Li, K. L. Wong, Y. Liu, G. Yin, and K. L. Wang, Spin-orbit torque from a ferromagnetic metal, *Phys. Rev. B* **99**, 184403 (2019).
- [93] P. M. Levy, Extraordinary Hall effect in Kondo-type systems: Contributions from anomalous velocity, *Phys. Rev. B* **38**, 6779 (1988).
- [94] B. Zimmermann, K. Chadova, D. Kodderitzsch, S. Blugel, H. Ebert, D. V. Fedorov, N. H. Long, P. Mavropoulos, I. Mertig, Y. Mokrousov, and M. Gradhand, Skew scattering in dilute ferromagnetic alloys, *Phys. Rev. B* **90**, 220403(R) (2014).
- [95] F. Töpler, A. Hönemann, K. Tauber, D. V. Fedorov, M. Gradhand, I. Mertig, and A. Fert, Nonlocal anomalous Hall effect in ternary alloys based on noble metals, *Phys. Rev. B* **94**, 140413 (2016).
- [96] J. Barnas, A. Fuss, R. E. Camley, P. Grünberg, and W. Zinn, Novel magnetoresistance effect in layered magnetic structures: Theory and experiment, *Phys. Rev. B* **42**, 8110 (1990).
- [97] J. Bass, CPP magnetoresistance of magnetic multilayers: A critical review, *J. Magn. Magn. Mater.* **408**, 244 (2016).
- [98] G. Y. Guo, S. Maekawa, and N. Nagaosa, Enhanced Spin Hall Effect by Resonant Skew Scattering in the Orbital-Dependent Kondo Effect, *Phys. Rev. Lett.* **102**, 036401 (2009).
- [99] B. Zimmermann, P. Mavropoulos, S. Heers, N. H. Long, S. Blügel, and Y. Mokrousov, Anisotropy of Spin Relaxation in Metals, *Phys. Rev. Lett.* **109**, 236603 (2012).
- [100] A. J. Berger, E. R. J. Edwards, H. T. Nembach, A. D. Karenowska, M. Weiler, and T. J. Silva, Inductive detection of fieldlike and dampinglike ac inverse spin-orbit torques in ferromagnet/normal-metal bilayers, *Phys. Rev. B* **97**, 094407 (2018).
- [101] M. Kawaguchi, D. Towa, Y.-C. Lau, S. Takahashi, and M. Hayashi, Anomalous spin-Hall magnetoresistance in Pt/Co bilayers, *Appl. Phys. Lett.* **112**, 202405 (2018).